SARS-CoV-2 nsp16 is regulated by host E3 ubiquitin ligases, UBR5, and MARCHF7

Li Tian[1#], Zongzheng Zhao[2#], Wenying Gao[1], Zirui Liu [2], Xiao Li[2*], Wenyan Zhang[1*] and Zhaolong Li[1*]

[1]Department of Infectious Diseases, Infectious Diseases and Pathogen Biology Center, Institute of Virology and AIDS Research, Key Laboratory of Organ Regeneration and Transplantation of The Ministry of Education, The First Hospital of Jilin University, Changchun 130000, Jilin, China

[2]Research Unit of Key Technologies for Prevention and Control of Virus Zoonoses, Chinese Academy of Medical Sciences, Changchun Veterinary Research Institute, Chinese Academy of Agricultural Sciences, Changchun 130000, Jilin, China

[#]These authors contributed equally to this article.

*Correspondence:

Wenyan Zhang (zhangwenyan@jlu.edu.cn), Xiao Li (skylee6226@163.com), and Zhaolong Li (lizhaolong@jlu.edu.cn)

Competing Interests: The authors declare no conflicts of interest.

Abstract

Severe acute respiratory syndrome coronavirus 2 (SARS-CoV-2), the virus responsible for coronavirus disease 2019 (COVID-19), remains a global public health threat with major economic implications. The non-structural protein 16 (nsp16) of SARS-CoV-2, in complex with nsp10, catalyses the final step of viral mRNA capping via its 2'-O-methylase activity, enabling the virus to evade host immunity and protect viral mRNA from degradation. However, host factors regulating nsp16 have not been thoroughly explored. Although various E3 ubiquitin ligases are known to interact with SARS-CoV-2 proteins, their specific roles in targeting nsp16 for degradation remain unclear. In this study, we demonstrate that nsp16 is ubiquitinated and degraded by host E3 ubiquitin ligases UBR5 and MARCHF7, acting through the ubiquitin-proteasome system (UPS). UBR5 and MARCHF7 induce nsp16 degradation via K48- and K27-linked ubiquitination, respectively, in independent processes that inhibit SARS-CoV-2 replication both in vitro and in vivo. Furthermore, UBR5 and MARCHF7 exhibited broad-spectrum antiviral activity by degrading nsp16 variants from different SARS-CoV-2 strains. Our findings uncover novel mechanisms by which the UPS antagonises SARS-CoV-2 replication and provide promising targets for therapeutic intervention against COVID-19.

Key words: SARS-CoV-2, nsp16, ubiquitination, UBR5, MARCHF7, proteasomal degradation

Introduction

Severe acute respiratory syndrome coronavirus 2 (SARS-CoV-2) has emerged as a global public health threat, causing over 700 million coronavirus disease 2019 (COVID-19) cases and 7 million deaths (Carabelli et al., 2023; Markov et al., 2023). SARS-CoV-2 encodes four structural proteins, 16 non-structural proteins (Nsps) that assist in viral replication and transcription, and a series of accessory proteins (ORFs) associated with immune evasion (V'kovski et al., 2021; Wang et al., 2020). Some viruses such as Ebola virus (Valle et al., 2021), dengue virus (Jung et al., 2018), and reovirus (Furuichi et al., 1975) encode 2'-O methyltransferases (2'-O-MTases) homologous to those found in eukaryotes. This allows them to mimic the host 5' cap structure on their RNA, hindering recognition by the innate immune system (Daffis et al., 2010; Züst et al., 2011). Similarly, SARS-CoV-2 nsp16, in complex with nsp10, functions as a 2'-O-MTase, methylating the first nucleotide of a capped viral RNA strand at the 2′-O position, converting the 5' cap of RNA from 'cap-0' to 'cap-1' (Benoni et al., 2021; Park et al., 2022). This modification shields SARS-CoV-2 from host antiviral responses such as MDA5 recognition and IFIT1 restriction (Bergant et al., 2022; Russ et al., 2022). Importantly, nsp16 inhibits global host mRNA splicing, which reduces host protein and mRNA levels (Banerjee et al., 2020). Additionally, nsp16 enhances SARS-CoV-2 cell entry by promoting TMPRSS2 expression (Han et al., 2023), highlighting its multifaceted role as a virulence factor. Moreover, nsp16-deficient strains exhibit reduced pathogenicity and induce a strong immune response, suggesting their potential as a live-attenuated vaccine candidate (Ye et al., 2022). Given nsp16's critical functions, drugs targeting nsp16 or the nsp16-nsp10 complex have been developed (Klima et al., 2022; Nguyen et al., 2022). Therefore, understanding host factors that interact with nsp16 is crucial for uncovering novel therapeutic strategies.

The ubiquitin-proteasome system (UPS) is an important pathway for the targeted degradation of intracellular proteins and is referred to as "the molecular kiss of death" (Dongdem & Wezena, 2021; Park et al., 2020). Substrate ubiquitination requires a cascade of three ligases: E1, E2, and E3 (Zheng & Shabek, 2017). Some E3 ubiquitin

ligases function as monomers, while others form multi-subunit E3 complexes. Regardless of their form, all E3 ligases share the same functional specificity in recognizing substrates and determining the specificity of the UPS. In some complexes, an additional protein may be required as a substrate receptor to recognize the substrate (Iconomou & Saunders, 2016; Yang et al., 2021). E3 ligases are indispensable for direct binding to substrates and determining the specificity of the UPS (Li et al., 2021; Wang et al., 2022). Researchers have identified over 600 human genome-encoded E3 ligases that operate in diverse cellular environments, respond to a wide range of cellular signals, and regulate a vast array of protein substrates (Dongdem & Wezena, 2021; Garcia-Barcena et al., 2020). Dysregulation of E3 ligase activity has been implicated in various human diseases, making them promising drug targets (Humphreys et al., 2021). E3 ligases are classified into three classes based on conserved domains and ubiquitin (Ub) transfer mechanisms: Really Interesting New Gene (RING) E3s, homologous to the E6AP carboxyl terminus (HECT) E3s, and RING-between-RING (RBR) E3s (Garcia-Barcena et al., 2020; Morreale & Walden, 2016). RING E3 ligases directly transfer Ub from the E2-Ub complex to the substrate (Deshaies & Joazeiro, 2009), whereas HECT-type E3s transfer Ub to their own catalytic cystine residue before attaching it to the substrate (Huibregtse et al., 1995). RBR E3s combine the characteristics of both RING and HECT types (Walden & Rittinger, 2018). RBR and RING E3s share the RING-binding domains, but RBR family members can generate thioester intermediates with Ub, as is the case with HECT-type E3s (Garcia-Barcena et al., 2020).

To investigate the relationship between SARS-CoV-2 and host factors, we focused on the interaction between nsp16 and the UPS. In this study, we present a novel regulatory mechanism targeting nsp16 via the host UPS. We demonstrate, for the first time, that nsp16 is ubiquitinated and degraded by the host proteasome. Interestingly, two E3 ligases from distinct families, the RING-type MARCHF7 and the HECT-type UBR5, independently recognise and target nsp16 for degradation in the cytoplasm and nucleus. Since nsp16 possesses 2'-O-MTase activity, its enzymatic function converts the viral RNA 5' cap structure from cap-0 to cap-1. This dual targeting of nsp16 by MARCHF7 and UBR5 leads

104 to its degradation, disrupting its function and ultimately demonstrating effective antiviral
105 activity against SARS-CoV-2. Our findings identify novel therapeutic targets for developing
106 effective strategies to prevent SARS-CoV-2 and treat COVID-19.
107

Results

Ubiquitination and proteasomal degradation of SARS-CoV-2 nsp16 by the UPS

Ubiquitination plays an important role in SARS-CoV-2 infection and pathogenesis (Gao et al., 2022; Guo et al., 2021; Li et al., 2023; Zhang et al., 2021; Zhang et al., 2024; Zhang et al., 2023). To explore whether the non-structural proteins of SARS-CoV-2 are regulated by the UPS, we examined the effect of the proteasome inhibitor MG132 on the protein expression of all 16 non-structural proteins. MG132 treatment markedly increased the abundance of nsp8, nsp11, and nsp16 proteins in HEK293T cells (Fig. 1A), suggesting their potential degradation by the UPS. It has been reported that nsp8 undergoes UPS-mediated degradation via TRIM22-mediated ubiquitination (Fan et al., 2024). In this study, we focused on nsp16 for further investigation. To confirm the role of the UPS in nsp16 degradation, we employed additional proteasome inhibitors, Bortezomib and Carfilzomib. Unlike the lysosomal inhibitors Bafilomycin A1 and NH_4Cl and the autophagy-lysosomal inhibitor vinblastine, these proteasome inhibitors enhanced nsp16 stability (Fig. 1B). The impact of the USP on the half-life of nsp16 was investigated. To this end, nsp16-expressing cells were treated with a protein synthesis inhibitor, cycloheximide, and the kinetics of nsp16 decay were examined. We observed that the half-life of nsp16 in MG132-treated samples was significantly longer than that in MG132-untreated samples (15 h versus 2 h) (Fig. 1C and 1D).

To identify proteins interacting with nsp16, we performed co-immunoprecipitation (Co-IP) followed by mass spectrometry (MS) analysis, comparing nsp16-expressing cells treated with and without MG132 (Fig. 1E). KEGG pathway and Gene Ontology analyses of the MS data (Figure 1—figure supplement 1A). Biological process enrichment analysis showed that blocking nsp16 degradation resulted in an increase in the number of proteins that interact with it, including 43 proteins involved in virus-associated processes and 22 proteins involved in regulating mRNA stability. Five proteins were related to the regulation of the cellular antiviral defence. Additionally, interactions were associated with mRNA splicing and RNA methylation (Banerjee et al., 2020), consistent with nsp16's role as a

136 2'-O-MTase. Furthermore, SARS-CoV-2 uses nsp16 to disrupt host mRNA splicing to
137 facilitate its infection (Park et al., 2022; Russ et al., 2022; Züst et al., 2011). These findings
138 corroborate the reliability of our MS data.

139 As expected, we found that several nsp16-binding proteins were related to
140 ubiquitination and degradation pathways (Figure 1 — figure supplement 1B). Four
141 deubiquitinases (DUBs), the E2 ligase UBE2D3, and 14 proteasomal enzymes were
142 identified. Of these, six E3 ligases, UBR5, MARCHF7, HECTD1, TRIM32, MYCBP2, and
143 TRIM21, were chosen for further investigation.

144 **E3 ligases UBR5 and MARCHF7 independently mediate nsp16 degradation**

145 To identify the E3 ligases responsible for nsp16 degradation, we designed small
146 interfering RNA (siRNA) targeting the six candidate E3 ligases and evaluated their effects
147 on nsp16 abundance. Knockdown of UBR5 and MARCHF7 stabilised the protein levels of
148 nsp16 (Fig. 2A). Furthermore, we generated stable cell lines with UBR5 or MARCHF7
149 knockdowns to further investigate their effects on nsp16 stability and confirm silencing
150 efficiency (Fig. 2B). To determine whether UBR5 and MARCHF7 cooperate in nsp16
151 degradation, we knocked down UBR5 or MARCHF7 using siRNA in MARCHF7- or
152 UBR5-knockdown cells, respectively. Knockdown of UBR5 in MARCHF7-knockdown cells,
153 and vice versa, further enhanced nsp16 stability. This indicates that UBR5 and MARCHF7
154 act independently to degrade nsp16 (Fig. 2C). We further validated the independent
155 function of these E3 ligases by examining nsp16 degradation. MARCHF7 overexpression
156 induced nsp16 degradation in both MARCHF7-knockdown and
157 MARCHF7/UBR5-double-knockdown cells. Similarly, UBR5 overexpression degraded
158 nsp16 even in the presence of MARCHF7 knockdown. Knockdown efficiencies were
159 confirmed for all experiments (Figure 2 — figure supplement 1A and 1B). Notably,
160 overexpression of wild-type MARCHF7 or UBR5, but not mutants lacking the functional
161 RING domain (1-542 aa) or the HECT domain inactivated mutant, disrupts the stability of
162 nsp16 in cells with MARCHF7 or UBR5 knockdown (Fig. 2D and 2E). These findings
163 demonstrate that UBR5 and MARCHF7 independently ubiquitinate nsp16 via their HECT

164 or RING domains, targeting it for proteasomal degradation.

165 **UBR5 and MARCHF7 mediate distinct Ub linkages on nsp16**

166 We first confirmed the ubiquitination of nsp16, both in the presence and absence of
167 exogenous Ub (Fig. 3A-B). To further investigate the regulation by E3 ligases, we
168 examined the impact of UBR5 or MARCH7 knockdown on nsp16 ubiquitination.
169 Knockdown of either UBR5 or MARCHF7 decreased the ubiquitination level of nsp16
170 compared to that in the negative control (Fig. 3C). Ub contains seven lysine residues (K6,
171 K11, K27, K29, K33, K49, and K63) that form polyubiquitin chains with distinct functions,
172 ultimately dictating the fate of the attached target protein (Grice & Nathan, 2016). To
173 determine the specific type of polyubiquitin chain modification of nsp16 mediated by UBR5
174 and MARCH7, we constructed a series of Ub mutants retaining only a single lysine
175 residue. Except for K33, all single-lysine Ub mutants promoted nsp16 ubiquitylation to
176 varying extents, suggesting a complex polyubiquitin chain structure on nsp16 potentially
177 regulated by multiple E3 ligases or E2-E3 ligase pairs (Fig. 3D). Notably, analysis of
178 specific lysine linkages revealed that MARCHF7 knockdown primarily reduced the
179 K27-linked ubiquitination of nsp16, while UBR5 knockdown primarily reduced the
180 K48-linked ubiquitination of nsp16 (Fig. 3E and 3F). These findings indicate that
181 MARCHF7 and UBR5 induce K27- and K48-linked ubiquitination on nsp16, respectively.

182 **UBR5 and MARCHF7 directly interact and colocalise with nsp16 in the endoplasmic**
183 **reticulum (ER)**

184 MS analysis suggested interactions between nsp16 and both UBR5 and MARCH7.
185 Co-IP experiments confirmed that both Myc-tagged MARCHF7 and endogenous UBR5
186 interact with nsp16 (Figure 4—figure supplement 1A and 1B). To determine whether
187 MARCHF7 or UBR5 directly interact with nsp16, fluorescence resonance energy transfer
188 (FRET) assays were performed. When nsp16-YFP was bleached, the fluorescence
189 signals from CFP-UBR5 or CFP-MARCHF7 fusion proteins increased, indicating a direct
190 interaction between these E3 ligases and nsp16 (Figure 4—figure supplement 1C). Image

191 J software was used to quantify the relative fluorescence intensities (Figure 4—figure
192 supplement 1D). We next investigated whether UBR5 and MARCHF7 require each other
193 for nps16 binding. We compared the binding ability of UBR5 to nsp16 in the presence or
194 absence of MARCHF7 using Co-IP. MARCHF7 knockdown had no effect on the
195 interaction between UBR5 and nsp16, and vice versa (Fig. 4A and 4B), indicating
196 independent binding of UBR5 and MARCHF7 to nsp16. Previous studies have shown that
197 nsp16 is localised to both the nucleus and cytoplasm (Zhang et al., 2020). UBR5
198 (containing two nuclear localisation signals) and MARCHF7 are present in both
199 compartments (Muñoz-Escobar et al., 2015; Shearer et al., 2018) (Nathan et al., 2008).
200 Immunofluorescence staining revealed that UBR5 and MARCHF7 colocalised primarily
201 with nsp16 in the cytoplasm, with some colocalisation in the nucleus of Hela cells (Figure
202 4—figure supplement 1E). Similar results were observed in nsp16-transfected HEK293T
203 cells using antibodies against endogenous UBR5 or MARCHF7 (Figure 4 — figure
204 supplement 1F).

205 To identify the specific cellular compartment where UBR5 or MARCH7 interacts with
206 nsp16, we co-transfected cells with UBR5-CFP or MARCH7-CFP along with nsp16-YFP.
207 Immunostaining was performed with organelle-specific antibodies to label the
208 mitochondrial marker COX5A, the ER marker PDI, and the Golgi apparatus marker
209 GM130. Notably, both UBR5 and MARCHF7 interacted with nsp16 and colocalised with
210 PDI, but not with COX5A or GM130 (Fig. 4C and 4D). These findings indicate that UBR5
211 and MARCHF7 directly interact with nsp16 in the ER.

212 **Functional domains of UBR5 and MARCHF7 are required for nsp16 interaction and**
213 **ubiquitination**

214 UBR5 is a four-domain E3 ligase containing two nuclear localisation signals. The four
215 domains are UBA, UBR, PABC, and HECT (Muñoz-Escobar et al., 2015) (Figure 4—figure
216 supplement 2A). Notably, the HECT domain is essential for its E3 ligase activity, where
217 UBR5 must be conjugated to Ub before transferring it to the substrate (Kim et al., 2021).
218 To identify the UBR5 domain responsible for nsp16 ubiquitination, we utilised UBR5

219 mutants with inactivated individual domains. Only the HECT domain mutant failed to
220 degrade nsp16 (Figure 4—figure supplement 2B), consistent with previous findings (Zhou
221 et al., 2022), and was unable to induce nsp16 ubiquitination, further supporting its
222 essential function (Figure 4—figure supplement 2C).

223 To identify the MARCHF7 region responsible for nsp16 degradation, we constructed a
224 series of truncation mutants, as previously described (Figure 4—figure supplement 2D)
225 (Zhao et al., 2018) (Nathan et al., 2008). All mutants lost the ability to degrade nsp16
226 (Figure 4—figure supplement 2E). Furthermore, we explored the ability of these mutants
227 to interact with nsp16 and their impact on nsp16 ubiquitination. Only the mutant with an
228 intact N-terminal region (aa 1–542) retained strong binding to nsp16, while mutants with
229 the active RING domain region (aa 543–616) did not. Consistently, only the wild-type
230 MARCHF7 induced the formation of K27-linked Ub chains on nsp16 (Figure 4—figure
231 supplement 2F). These findings suggest that the N-terminal of MARCH7 mediates binding
232 to nsp16, while the RING domain is required for its K27-linked ubiquitination activity.

233 **UBR5 and MARCHF7 mediate antiviral activity against SARS-CoV-2 by targeting**
234 **nsp16 for degradation**

235 To examine the functional impact of nsp16 degradation by UBR5 and MARCHF7 on
236 viral replication, we used a biosafety level 2 cell culture system to generate SARS-CoV-2
237 transmissible virus-like particles capable of infecting and replicating in Caco2-N^{int} cells (Ju
238 et al., 2021). Knockdown of either UBR5 or MARCHF7 in these cells significantly
239 increased SARS-CoV-2 replication compared with that in the control group. Notably,
240 simultaneous knockdown of both UBR5 and MARCHF7 further increased SARS-CoV-2
241 replication (Figure 5—figure supplement 1A and 1B).

242 Given the critical antiviral roles of UBR5 and MARCH7, we investigated the
243 modification of nsp16 following viral infection. HEK293T cells stably expressing the
244 SARS-CoV-2 entry receptor ACE2 (HEK293T-ACE2) were infected with the Wuhan strain
245 for 48 h. Co-IP using an anti-nsp16 antibody revealed that nsp16 interacts with

246 endogenous MARCHF7 and UBR5 and undergoes ubiquitination (Fig. 5A). We further
247 validated the antiviral effects of UBR5 and MARCH7 in a biosafety level 3 facility using the
248 Wuhan strain at a multiplicity of infection (MOI) of 0.01 and the Omicron strain at an MOI
249 of 0.001. Compared to the control group, UBR5 or MARCH7 knockdown in Caco2 cells
250 significantly increased intracellular and secreted viral mRNA levels (*M* and *E* genes) of
251 both strains. Additionally, with the Wuhan strain, MARCH7 knockdown resulted in a
252 0.6-log increase in viral titre in the supernatants, while UBR5 knockdown caused an over
253 1-log increase. With the Omicron strain, knockdown of the two E3 ligases resulted in an
254 even greater increase in viral titres (Fig. 5C–E for the Wuhan strain and 5F–H for the
255 Omicron strain). Immunoblotting (IB) confirmed these findings, demonstrating elevated
256 intracellular and secreted N protein levels upon UBR5 or MARCH7 knockdown (Fig. 5I).
257 The knockdown efficiency of MARCHF7 and UBR5 was also confirmed (Fig. 5B). Due to
258 low transfection efficiency in Caco2 cells, we overexpressed UBR5-Myc or MARCH7-Myc
259 in HEK293T-ACE2 cells. Overexpression of UBR5 or MARCH7 significantly decreased
260 viral mRNA levels of the *M* and *E* genes in both the Wuhan and Omicron strains, as
261 measured by real-time quantitative polymerase chain reaction (RT-qPCR). IB analysis
262 also showed decreased N protein levels in cells and supernatants, accompanied by a
263 decrease in viral titres of more than 0.5-log. However, co-transfection with increasing
264 amounts of nsp16 significantly abrogated the inhibitory effects of UBR5 and MARCH7 on
265 SARS-CoV-2 replication (Fig. 6A–H and Figure 6—figure supplement 1A–H). To eliminate
266 the potential influence of nsp16's intrinsic function on experimental outcomes, we
267 overexpressed UBR5 with an inactive HECT domain (UBR5-ΔHECT) or MARCHF7 with a
268 RING domain deletion (MARCHF7-1-542), along with nsp16. These E3 ligase mutants
269 failed to inhibit viral replication. Moreover, a gradual enhancement of nsp16 protein
270 expression did not enhance viral replication. While there was a slight increase in the
271 mRNA levels of *M*, protein levels of E and N remained unchanged (Figure 6—figure
272 supplement 2A–H). These results suggest that UBR5 and MARCH7 exhibit antiviral
273 activity against SAR-CoV-2 of UBR5 and MARCHF7 through their enzymatic function,

274 significantly suppressing viral replication by targeting nsp16 for degradation.

275 **UBR5 and MARCHF7 mediate broad-spectrum degradation of nsp16 variants**

276 Given the ongoing emergence of SARS-CoV-2 variants, broad-spectrum antiviral
277 activity remains critical. To investigate whether UBR5 and MARCH7 can mediate
278 broad-spectrum degradation of various nsp16 variants, we aligned the amino acid
279 sequences of nsp16 proteins obtained from the National Center for Biotechnology
280 Information (Figure 6 — figure supplement 3A). Among these, only three variants,
281 XBB.1.9.1, XBB.1.5, and XBB.1.16, exhibited a higher number of mutation sites compared
282 to other variants, which showed only one or two mutations, suggesting a more conserved
283 sequence. Consequently, using mutagenesis techniques, we synthesised the nsp16
284 sequences for these three variants along with several single-site mutants from other
285 variants. Treatment with the proteasome inhibitor MG132 restored nsp16 protein levels for
286 all variants (Figure 6—figure supplement 3B), confirming that degradation occurs through
287 the UPS. Furthermore, knockdown of either UBR5 or MARCHF7 increased the stability of
288 nsp16 proteins from these variants, albeit to varying degrees, indicating that these nsp16
289 proteins are sensitive to UBR5- or MARCHF7-mediated degradation (Figure 6 — figure
290 supplement 3C). Taken together, these findings suggest that UBR5 and MARCHF7 may
291 confer broad-spectrum antiviral activity by targeting nsp16 from diverse SARS-CoV-2 for
292 degradation.

293 **SARS-CoV-2 infection reduces UBR5 and MARCHF7 expression**

294 To explore the relationship between SARS-CoV-2 infection and the expression levels
295 of UBR5 and MARCHF7, we analysed changes in their mRNA and protein levels after
296 infection with either the Wuhan or Omicron strains at varying MOIs, using RT-qPCR and
297 IB, respectively. Both mRNA and protein levels of MARCFH7 decreased with increasing
298 viral titres. However, UBR5 expression initially increased at low titres but continuously
299 declined with increasing titres (Figure 6 — figure supplement 4A-4C). Previous studies
300 have reported a role for UBR5 in regulating interferon-γ-mediated pathways, which might

301 explain the observed increase in UBR5 expression at low titres (Wu et al., 2022). To
302 confirm these findings *in vivo*, we examined UBR5 and MARCHF7 mRNA levels in
303 peripheral blood mononuclear cells from SARS-CoV-2-infected patients with varying
304 disease severity. While UBR5 mRNA levels negatively correlated with disease
305 progression, MARCHF7 levels showed no significant correlation (Figure 6 — figure
306 supplement 4D). These results suggest that SARS-CoV-2 may suppress host antiviral
307 defences mediated by UBR5 and MARCHF7.

308 **UBR5 and MARCHF7 protect mice from SARS-CoV-2 challenge**

309 Given the lack of known activators or inhibitors for E3 ligases, we developed a
310 transient overexpression method for UBR5 and MARCH7 in mice using high-pressure tail
311 vein injection of plasmids (Bonamassa et al., 2011). To assess their *in vivo* antiviral effects,
312 mice were injected with plasmids encoding UBR5 or MARCH7, followed by SARS-CoV-2
313 challenge (Fig. 7A). Both MARCHF7 and UBR5 overexpression significantly decreased
314 viral *E* gene copy numbers in mouse lungs compared to those in the control group, as well
315 as markedly decreased viral titres in lung tissue homogenates (Fig. 7C-D). Additionally,
316 treated mice experienced less weight loss (Fig. 7E). Histopathological analysis of major
317 organs 5 d post-infection revealed that lungs from mice treated with UBR5 or MARCH7
318 displayed attenuated lesions, including alveolar contraction and pulmonary oedema,
319 compared to those typically observed in control mice (Fig. 7F). These treatments also
320 reduced the abundance of N proteins (Fig. 7G). Collectively, these results suggest that
321 UBR5 or MARCH7 overexpression inhibits SARS-CoV-2 virulence *in vivo* by promoting
322 nsp16 protein degradation.

323 SARS-CoV-2 infection can trigger a severe cytokine storm, thought to be responsible
324 for its high mortality rates (Song et al., 2020) (Hojyo et al., 2020). To examine the effect of
325 UBR5 and MARCH7 on inflammatory responses, we measured levels of key cytokines,
326 including interleukin-6, interleukin-1 receptor antagonist, and interleukin-1β, in the spleens
327 of SARS-CoV-2-infected mice (Makaremi et al., 2022) (Hu et al., 2021). Consistent with
328 their antiviral activity, treatment with UBR5 or MARCH7 significantly reduced the

329 production of these cytokines (Fig. 7H).

330

331 **Discussion**

332 SARS-CoV-2 nsp16 functions as a 2'O-MTase, catalysing the methylation of the
333 penultimate nucleotide of the viral RNA cap. This modification produces a 5'-RNA cap
334 structure that mimics host RNA, thereby evading host immune detection and responses
335 (Lin et al., 2020) (Balieiro et al., 2022; Russ et al., 2022). High-resolution structures of
336 nsp16 and nsp16-nsp10 heterodimers have been characterised (Rosas-Lemus et al.,
337 2020) (Klima et al., 2022; Lugari et al., 2010), paving the way for antiviral drug
338 development targeting these heterodimers (Balieiro et al., 2022; Melo-Filho et al., 2022).
339 However, the host factors that interact with and regulate nsp16 remain largely unknown.

340 Previously, our group and others have demonstrated the importance of the UPS in
341 modulating SARS-CoV-2 infection (Xu et al., 2022). For example, host E3 ligases, such as
342 RNF5, Cullin4-DDB1-PRPF19, ZNF598, and TRIM7, ubiquitinate and degrade key
343 SARS-CoV-2 proteins, thereby suppressing viral replication (Li et al., 2023; Liang et al.,
344 2022; Maimaitiyiming et al., 2022; Zhang et al., 2024). Conversely, SARS-CoV-2 employs
345 DUBs to counteract these host defences and enhance its replication (Chen et al., 2024;
346 Gao et al., 2024; Gao et al., 2022; Guo et al., 2021). In this study, we identify nsp16 as a
347 short-lived protein with a half-life of only 2–3 h that is targeted for ubiquitination and
348 degradation by the UPS. Using MS and bioinformatics screening, we identified two E3
349 ligases, UBR5 and MARCHF7, that directly interact with and target nsp16 for
350 ubiquitination and degradation.

351 UBR5 is a member of the UBR box protein family and contains a HECT domain
352 essential for its E3 ligase activity (Kim et al., 2021). It is known to regulate tumour growth,
353 metastasis (Xiang et al., 2022) (Qiao et al., 2020), and viral infections. For example, URB5
354 targets Middle East respiratory syndrome coronavirus ORF4b protein for degradation,
355 dampening the host immune response (Zhou et al., 2022). Conversely, UBR5 acts as a

356 cofactor for Zika virus replication by helping TER94/VCP degrade the capsid protein to
357 expose the viral genome to the cytoplasm (Gestuveo et al.). MARCHF7 is a RING E3 Ub
358 ligase that regulates T cell proliferation, neuronal development, inflammasomes, and
359 tumour progression (Zheng, 2021) (Zhang et al., 2016) (Cai et al., 2022) (Zhao et al.,
360 2018). However, its role in viral infections has been largely unexplored, with only one
361 study identifying it as a host protein interacting with the 2C of foot-and-mouth disease
362 virus (Mahajan et al., 2021).

363 Our findings reveal that UBR5 and MARCHF7 independently interact with nsp16 and
364 facilitate its degradation, primarily within the cytoplasmic side of the ER. This reflects an
365 evolutionary arms race between viruses, which develop mechanisms to resist host
366 antiviral responses, and hosts, which deploy multiple strategies to counteract the virus.
367 One such strategy is seen with multiple E3 ligases that target the same viral protein for
368 degradation. Functional analyses demonstrate that UBR5 or MARCHF7 knockdown
369 enhanced SARS-CoV-2 replication, whereas their overexpression impaired replication.
370 Furthermore, we found that when the enzymatic activity of these E3 ligases is inactivated,
371 their antiviral effect is abolished, indicating that their antiviral effects are dependent on
372 their E3 ligase activity. Additionally, we observed that in the absence of functional UBR5 or
373 MARCH7, overexpression of nsp16 does not increase viral levels. This suggests that
374 although nsp16 plays an important role, it cannot independently promote viral replication
375 without the involvement of E3 ligases. This underscores the critical function of UBR5 and
376 MARCHF7 as antiviral factors that suppress SARS-CoV-2 replication by promoting nsp16
377 degradation.

378 Notably, while nsp16 possesses 18 lysine residues, identifying specific ubiquitination
379 sites proved challenging. Based on structural data of nsp16 (Decroly et al., 2011), we
380 constructed truncated nsp16 mutants to assess their degradation profiles. We found that
381 nsp16 could still be degraded to varying degrees (Appendix-figure S2A-B), suggesting
382 that multiple lysine residues serve as recognition sites for E3 ligases. Nonetheless, the
383 results from these truncated mutants regarding the MG132 recovery provided us with
384 valuable insights. For instance, the Δ2-17 mutant, which lacks this segment, showed more

385 than a two-fold increase in nsp16 expression levels. Conversely, the Δ204-212 mutant
386 exhibited significantly reduced recovery after MG132 treatment compared to the wild-type.
387 These observations offer important clues for further investigation into the interaction
388 regions between nsp16 and MARCHF7 or UBR5, as well as potential ubiquitination sites.
389 MS analysis identified K76 of nsp16 as a ubiquitination site (Appendix-figure S2C).
390 However, an nsp16 K76R mutant was still degraded by E3 ligases, although the degree of
391 ubiquitination was reduced compared to that of the wild-type, indicating that K76 might be
392 one of several potential ubiquitination sites (Appendix-figure S2D-E). Therefore, we
393 hypothesise that nsp16 undergoes ubiquitination at multiple sites and may involve
394 non-canonical ubiquitination pathways at non-lysine residues (McClellan et al., 2019). A
395 comprehensive understanding of the ubiquitination landscape of nsp16 requires further
396 investigation. In addition to UBR5 and MARCHF7, other E3 ligases could contribute to
397 nsp16 regulation, which warrants further studies.

398 Currently, no specific activators or inhibitors exist for UBR5 or MARCH7. To validate
399 their antiviral effects *in vivo*, we employed high-pressure tail vein injection, a method
400 commonly used for gene delivery to the liver (Kamimura et al., 2014). This method has
401 also been shown to facilitate gene delivery to other tissues, including the lungs
402 (Bonamassa et al., 2011). Gene expression was successfully detected in lung tissues.
403 While this method induced mild immune activation, its effect is relatively minimal
404 compared with that of other techniques (Suda et al., 2023). Moreover, studies suggest that
405 mice and non-human primates exhibit higher resistance to innate immune activation than
406 humans, suggesting that our findings were only minimally influenced by immune activation
407 (Raper et al., 2003). However, this highlights that translating new drug targets into
408 therapeutic treatments will require considerable time and effort. For example, human trials
409 involving the injection of naked DNA (e.g., OTC cDNA) have shown variable outcomes.
410 While no severe immune responses were observed in most participants, one case of fatal
411 immune activation was reported (Raper et al., 2003), highlighting the variability of human
412 immune responses and a key limitation in extrapolating findings from animal models to
413 human trials. This variability might also explain why we did not observe a clear trend for

414 MARCHF7 mRNA levels in peripheral blood samples from patients with varying disease
415 severities. The limited number of patients in our study could further contribute to this
416 observation.
417 In this study, we identified the host E3 ligases, UBR5 and MARCHF7, as critical regulators
418 of SARS-CoV-2 nsp16 through ubiquitination and subsequent degradation. We
419 demonstrated a negative correlation between the expression levels of these ligases and
420 the degree of infection, underscoring their antiviral roles. Furthermore, both ligases
421 significantly inhibit SARS-CoV-2 replication. Our findings pave the way for the
422 development of novel therapeutic strategies targeting the UPS for the treatment of
423 COVID-19.

424 **Materials and Methods**

425 **Reagents and antibodies**

426 The drugs used in this study were as follows: MG132 (catalog no. S2619),
427 Bafilomycin A1 (catalog no. S1413), Bortezomib (catalog no. S1013), Carfilzomib (catalog
428 no. S2853) and Vinblastine (catalog no. S4504) were purchased from Selleck (Houston,
429 TX, USA). Cycloheximide (catalog no. 66-81-9) was purchased from Sigma (Saint Louis,
430 MO, USA). The antibodies used for immunoblotting analysis (IB) were as follows:
431 anti-UBR5 mAb (Proteintech, Rosemont, IL, USA, catalog no. 66937-1-Ig),
432 anti-MARCHF7 mAb (Santa Cruz Biotechnology, Dallas, TX , USA, catalog no.
433 sc-166945), SARS-CoV-2 2'-O-ribose Methytransferase Antibody (nsp16) (Cell signaling,
434 Danvers, Massachusetts, USA, catalog no. #70811), anti-Flag mAb (Sigma, catalog no.
435 F1804), anti-tubulin mAb (Abcam, Cambridge, Cambridgeshire, UK, catalog no. ab11323),
436 anti-hemagglutinin (anti-HA) pAb (Invitrogen, catalog no. 71-5500), anti-Myc pAb
437 (Proteintech, Rosemont, IL, USA, catalog no. 16286-1-AP), and anti-GFP mAb (Abcam,
438 catalog no. ab1218). Primary antibody: anti-COX5A pAb (Sangon Biotec, Shanghai, CHN,
439 catalog no. D261450), anti-PDI-mAb (Proteintech, catalog no. 2E6A11) and Human
440 GM130/GOLGA2 Antibody (R&D Systems, Minneapolis, MN, USA, catalog no. AF8199)
441 were used for immunofluorescence, and SARS-CoV-2 nucleocapsid monoclonal antibody
442 (mAb) (GeneTex, Irvine, CA, USA, catalog no. GTX635679) were used for

443 Immunohistochemistry. Fluorescent secondary antibodies: goat anti-Rabbit IgG (H+L)
444 Highly Cross Adsorbed Secondary Antibody, Alexa Fluor Plus 488 (Invitrogen, catalog no.
445 A11001), and goat anti-Rabbit IgG (H+L) Highly Cross Adsorbed Secondary Antibody,
446 Alexa Fluor Plus 568 (catalog no. A-11011) and immunohistochemical secondary
447 antibodies: Streptavidin-Peroxidase Anti-Rabbit IgG kit (catalog no. KIT-9706) were
448 purchased from Invitrogen and maixin (Fuzhou, CHN) respectively.

449 **Cell lines and viruses**

450 The cell lines used in this study include HEK293T cells (catalog no. CRL-11268), Hela
451 cells (catalog no.CRM-CCL-2), Caco2 cells (catalog no. HTB-37). All cell lines were
452 purchased from American Type Culture Collection (ATCC; Manassas, VA, USA) and
453 tested for mycoplasma. In order to conduct virus related experiments, stable cell lines
454 including Caco2-N^{int} (stably expressing SARS-CoV-2 N gene) and 293T-ACE2 (stably
455 expressing ACE2) were generated in our laboratory. The cells were cultured in a cell
456 incubator containing 5% CO2 at 37°C using Dulbecco's modified Eagle's medium (DMEM;
457 HyClone, Logan, UT, USA) containing 10% heat-inactivated fetal calf serum (FCS, GIBCO
458 BRL, Grand Island, NY, USA), 100 mg/ml penicillin, and 100 ug/ml streptomycin to provide
459 nutrition. We expanded SARS-CoV-2 virus-like-particles (Wuhan-Hu-1, MN908947,
460 Clade:19A) with high replication capacity in Caco2-N^{int} using a biosafety level-2 (BSL-2)
461 cell culture system. The virus infecting the cells include Omicron BA. 1 strain
462 (human/CHN_CVRI-01/2022) and SARS-CoV-2 Wuhan strain
463 (BetaCoV/Beijing/IME-BJ05-2020, GenBank access no. MT291831.1), and mouse
464 adapted SARS-CoV-2/C57MA14 variant (GenBank: OL913104.1) used for experiments in
465 mice were provided by Key Laboratory of Jilin Province for Zoonosis Prevention and
466 Control, and all experiments for virus infection were performed in Biosafety level 3 (BSL-3)
467 cell culture system.

468 **Plasmids**

469 Eukaryotic expression plasmids encoding SARS-CoV-2 nsp protein were provided by
470 Professor Wang Peihui (Shandong University). The nsp16-HA expression vector was
471 constructed by adding HA tag at the C-terminus. UBR5 (Gnen ID: 51366) and its mutants

472 (UBR5-ΔHECT, UBR5-ΔPABC, UBR5-ΔUBR) expression plasmids were constructed
473 using purchased plasmids from Addgene (Watertown, MA, USA) as templates with no tag
474 or a MYC tag at the N-terminus. The cDNA of 293T cells was used as a template to
475 construct MARCHF7(Gene ID: 64844) and its truncated mutant with a Myc tag at the
476 C-terminus. All the above expression plasmids were inserted into the VR1012 vector. For
477 immunofluorescence (IF) and Fluorescence Resonance Energy Transfer (FRET)
478 experiments, pCDNA3.1-YFP vector (catalog no. 13033) and pECFP-C1 vector (catalog
479 no. 6076-1) were purchased from Addgene and BD (Biosciences Clontech), and
480 MARCHF7 or UBR5 was constructed on pECFP-C1, and nsp16 was constructed on
481 pCDNA3.1-YFP. Single point mutants of nsp16 of different virus subtypes were obtained
482 by point mutagenesis. Multi-site combined mutants were synthesized by Sangon Biotec
483 Company. Human ubiquitin protein and its mutants have been previously described.
484 Primers required for PCR were listed in Appendix Table S1.

485 **RNA extraction and real-time quantitative PCR**

486 We used the way of Trizol (Invitrogen, catalog no. 15596018CN) to extract RNA. The
487 RNA was subsequently reverse transcribed using a High-Capacity cDNA Reverse
488 Transcription kit (Applied Biosystems, Carlsbad, CA, USA, catalog no. 4368814). Finally,
489 PrimeScript RT Master Mix (Takara, Shiga, JPN, catalog no. RR036A) and relative
490 real-time primer were used for qPCR on an Mx3005P instrument (Agilent Technologies,
491 Stratagene, La Jolla, CA, USA). Amplification procedure of the target fragment is as
492 follows: predenaturation at 95°C for 2min, denaturation at 95 °C for 30s, annealing at
493 55 °C for 30s, and extension at 72 °C for 30s, total of 40 cycles. Real-time primer
494 sequences used in this study were shown in appendix table S1.

495 **Immunoblotting analysis (IB)**

496 Cells or supernatant cultured for a certain time were collected, cell precipitates were
497 resuspended with lysis buffer (50 mM Tris–HCl [pH 7.8], 150 mM NaCl, 1.0% NP-40, 5%
498 glycerol and 4 mM EDTA), 4xloading buffer was added (0.08M Tris [pH 6.8], 2.0%SDS,
499 10% glycerol, 0.1 M dithiothreitol, and 0.2% bromophenol blue), and samples were lysed
500 by heating at 100℃ for 30min. After removal of cell debris by centrifugation, the

501 supernatant was taken to separate proteins of different sizes by SDS-PAGE. The proteins
502 were transferred onto polyvinylidene fluoride (PVDF) membranes, incubated overnight
503 with the indicated primary antibody, and after 1 hour at room temperature with
504 HRP-conjugated secondary antibodies (Jackson Immunoresearch, West Grove, NJ, USA,
505 catalog no. 115-035-062 for anti-mouse and 111-035-045 for anti-rabbit), the proteins
506 were visualized through Ultrasensitive ECL Chemiluminescence Detection Kit
507 (Proteintech, catalog no. B500024).

508 **Stable cell line generation**

509 We purchased the lentiviral vector pLKO.1-puro (catalog no. 8453) from Adggen.
510 ShRNA targeting target genes were designed and synthesized by Sangon Biotech. After
511 annealing, it was inserted into the vector. Lentivirus was generated by transfection with
512 shRNA (cloned in pLKO.1) or control vector, RRE, VSVG and REV, and the cells were
513 screened with 1/1000 puromycin (3 μg/ml, Sigma, catalog no. P8833) after infection 48
514 hours. The knockdown efficiency was detected by RT-qPCR or IB. The shRNA target
515 sequences used in this study are shown in appendix table S1.

516 **RNAi**

517 Short interfering RNA (siRNA) used in this study were purchased from RiboBio Co.
518 Ltd. (Guangzhou, CHN). The siRNA sequences for knockdown of MARCHF7 or UBR5 are
519 provided in appendix table S1. The siRNA was transfected into the cells by transfection
520 reagent Lipofectamine 2000 (Invitrogen, catalog no. 11668-019), and the corresponding
521 plasmids were transfected 24 hours later using Lipofectamine 3000 Reagent (Invitrogen,
522 Carlsbad, CA, USA, catalog no. L3000-008). The expression of target genes was detected
523 by RT-qPCR or immunoblotting (IB) analysis 48 hours later.

524 **Immunoprecipitation**

525 After 10 hours of MG132 (10 μM) treatment, the cells were harvested, resuspended
526 in 1ml lysis buffer (50 mM Tris-HCl [pH 7.5], 150 mM NaCl, 0.5% NP-40) containing
527 protease inhibitor (Roche, catalog no. 11697498001), placed on the shaker oscillator for 4
528 hours to lyse, then centrifuged to remove cell debris, and the supernatant was incubated

529 with the antibody and protein G agarose beads (Roche, Basel, Basel-City, CH, catalog no.
530 11243233001) at 4°C overnight. Protein G agarose beads was washed 6-8 times with
531 wash buffer (20 mM Tris-HCL [pH 7.5], 100 mM NaCl, 0.1 mM EDTA, and 0.05% Tween
532 20) at 4°C, centrifuged at 800 g for 1 min. The proteins were eluted by adding loading
533 buffer (0.08 M Tris [pH 6.8], 2.0% SDS, 10% glycerol, 0.1 M dithiothreitol, and 0.2%
534 bromophenol blue), the samples were boiled at 100°C for 10min to elate the proteins. The
535 lysates and immunoprecipitations were detected by IB.

536 **Mass spectrometry (MS)**

537 HEK293T were transfected with SARS-CoV-2-nsp16-Flag for 36 hours, and then
538 harvested after 10 hours of treatment with MG132 or DMSO. Proteins were enriched by
539 co-immunoprecipitation assay. And the elutions were analyzed by MS. MS analysis was
540 performed by the national center for protein science (Beijing, CHN).

541 **Immunofluorescence**

542 At 48 hours after transfection, the solution was discarded and cells were washed
543 twice with preheated PBS for 5min each, followed by fixation with 4% paraformaldehyde
544 at 37°C for 10min. After three washes with PBS, permeabilized with 0.2% Triton X-100 for
545 5 min at 37°C, and then immediately followed by blocking with 10% fetal bovine serum at
546 room temperature for 1 hour. The blocked cells were incubated overnight with the
547 indicated primary antibodies. The next day, after three washes with PBS, the cells were
548 incubated with corresponding secondary antibodies for 1 hour at room temperature in the
549 dark. The nuclei were stained with DAPI (49,6-diamidino-2-phenylindole, Sigma, catalog
550 no. 9542) and then stored in 90% glycerol. The fluorescence was detected by a laser
551 scanning confocal microscope (FV 3000, Olympus, Tokyo, Japan).

552 **Viral infectivity assay**

553 The Caco2 cells were transfected with siRNA by Lipofectamine RNAiMAX Reagent
554 (Invitrogen, catalog no. 13778150) to knockdown UBR5 or MARCHF7 and infected with
555 Wuhan strain (MOI=0.01) or Omicron-BA.1 strain (MOI=0.001) at 24 hours after
556 transfection. After two hours of infection, the Caco2 cells were cultured in fresh medium
557 containing 2% fetal bovine serum for 48 hours. The cells and supernatants were collected.

558 Viral levels were characterized by RT-qPCR and IB analysis of viral structural proteins.
559 The overexpression plasmid UBR5-Myc, MARCHF7-Myc and nsp16-Flag was transfected
560 in 293T-ACE2 by Lipofectamine 3000 Reagent and infected with virus 24 hours later.

561 **Mouse lines and infections**

562 BALB/C mice, 6 weeks, were purchased from Charles River Laboratories, Beijing.
563 Mice were cultured in groups according to experimental groups. Our study examined male
564 and female animals, and similar findings are reported for both sexes. To reduce animal
565 suffering, all welfare and experimental procedures were carried out in strict accordance
566 with the Guide for the Care and Use of Laboratory Animals and relevant ethical
567 regulations during the experiment. The mice were randomly divided into 6 groups and
568 injected with 40 μg/500 μl MARCHF7 or UBR5 plasmids via the tail vein at high pressure.
569 Three groups of mice were infected 50ul with SARS-CoV-2 isolates by nasal challenge at
570 a dose of $10^{5.5}$ $TCID_{50}$/mL, three groups were not infected with virus as control, and the
571 empty vector injection group was also used as control.

572 **Immunohistochemical analysis**

573 Three mice in each group, a total of 18 mice, were sacrificed after anesthesia. The
574 lungs of mice were collected and fixed in 4% paraformaldehyde fixative. After 2 days, the
575 lungs were progressively dehydrated through different concentrations of ethanol solution,
576 transparently treated, soaked in xylene, and finally embedded in paraffin. Some thin
577 sections obtained through a microtome for hematoxylin and eosin (H&E) staining. The
578 other fraction was incubated with 3% hydrogen peroxide for 5-10 min at room temperature
579 to eliminate endogenous peroxidase activity. SARS-CoV-2 nucleocapsid monoclonal
580 antibody (mAb) (GeneTex, catalog no. GTX635679) and a Streptavidin-Peroxidase
581 Anti-Rabbit IgG kit (Maixin, Fuzhou, CHN, catalog no. KIT-9706) was used to quantify the
582 viral level in lung tissue.

583 **Statistical analysis**

584 The statistical analyses used in the figures have been described in detail in the figure
585 legends. All data were expressed as mean ± standard deviations (SDs). Statistical
586 comparisons were performed using student's t-test, one-way ANOVA, or repeated

587 measurement ANOVA. The differences were statistically significant as follows: *P < 0.05,
588 **P < 0.01, ***P < 0.001; ns is for no meaning

589 **Ethics statement**

590 Collection of inpatient blood was approved by the Ethics Committee of the First
591 Hospital of Jilin University (21K105-001) in accordance with the guidelines and principles
592 of WMA Declaration of Helsinki and the Department of Health and Human Services
593 Belmont Report. All study participants signed an informed consent form. PBMCS were
594 obtained from 9 COVID-19 patients with mild disease, 6 patients with severe disease, and
595 5 patients with critical disease (Appendix table S2). All animal experiments were approved
596 by the ethics committee of Research Unit of Key Technologies for Prevention and Control
597 of Virus Zoonoses, Chinese Academy of Medical Sciences, Changchun Veterinary
598 Research Institute, Chineses Academy of Agricultural Sciences (IACUC of
599 AMMS-11-2020-006).

600 **Acknowledgments**

601 We thank C.Y. Dai for providing critical reagents.

602 **Funding information**

603 This work was supported by funding from the National Natural Science Foundation of
604 China (82341072, 81930062 and 82272316 to ZWY, 82341062 to LZL), the National Key
605 R&D Program of China (2021YFC2301900 and 2301904, 2023YFC2306603), the
606 Science and Technology Department of Jilin Province (YDZJ202301ZYTS521 and
607 YDZJ202201ZYTS587), the Key Laboratory of Molecular Virology, Jilin Province
608 (20102209), and Bethune Project, Jilin University (2023B03). The funding sources were
609 involved in study design, data collection and interpretation, and the decision to submit
610 the work for publication.

611 **Authors' contributions**

612 L.T.: Conceptualization; Data curation; Formal Analysis; Investigation; Methodology;
613 Writing – original draft. Z.Z.: Methodology; Data curation; Writing – review & editing. Z.L.:
614 Conceptualization; Data curation; Formal Analysis; Investigation; Methodology; Writing –
615 review & editing; Funding acquisition. X.L., Z.L. and W.G.: Methodology; Resources. W.Z.:

Conceptualization; Formal Analysis; Funding acquisition; Methodology; Project administration; Resources; Writing – review & editing.

Data availability

The authors declare that [the/all other] data supporting the findings of this study are available within the paper [and its supplementary information files]. The mass spectrometry proteomics data have been deposited to the ProteomeXchange Consortium (http://proteomecentral.proteomexchange.org) via the iProX partner repository with the dataset identified PXD053961.

References

Balieiro, A. M., Anunciação, E. L., Costa, C. H., Qayed, W. S., & Silva, J. R. A. (2022). Computational Analysis of SAM Analogs as Methyltransferase Inhibitors of nsp16/nsp10 Complex from SARS-CoV-2. *International Journal of Molecular Sciences*, *23*(22), 13972.

Banerjee, A. K., Blanco, M. R., Bruce, E. A., Honson, D. D., Chen, L. M., Chow, A., Bhat, P., Ollikainen, N., Quinodoz, S. A., & Loney, C. (2020). SARS-CoV-2 disrupts splicing, translation, and protein trafficking to suppress host defenses. *Cell*, *183*(5), 1325-1339. e1321.

Bonamassa, B., Hai, L., & Liu, D. (2011). Hydrodynamic gene delivery and its applications in pharmaceutical research. *Pharm Res*, *28*(4), 694-701. https://doi.org/10.1007/s11095-010-0338-9

Cai, B., Zhao, J., Zhang, Y., Liu, Y., Ma, C., Yi, F., Zheng, Y., Zhang, L., Chen, T., & Liu, H. (2022). USP5 attenuates NLRP3 inflammasome activation by promoting autophagic degradation of NLRP3. *Autophagy*, *18*(5), 990-1004.

Chen, X., Tian, L., Zhang, L., Gao, W., Yu, M., Li, Z., & Zhang, W. (2024). Deubiquitinase USP39 promotes SARS-CoV-2 replication by deubiquitinating and stabilizing the envelope protein. *Antiviral Res*, *221*, 105790. https://doi.org/10.1016/j.antiviral.2023.105790

Decroly, E., Debarnot, C., Ferron, F., Bouvet, M., Coutard, B., Imbert, I., Gluais, L., Papageorgiou, N., Sharff, A., & Bricogne, G. (2011). Crystal structure and functional analysis of the SARS-coronavirus RNA cap 2′-O-methyltransferase nsp10/nsp16 complex. *PLoS pathogens*, *7*(5), e1002059.

Fan, L., Zhou, Y., Wei, X., Feng, W., Guo, H., Li, Y., Gao, X., Zhou, J., Wen, Y., Wu, Y., Shen, X., Liu, L., Xu, G., & Zhang, Z. (2024). The E3 ligase TRIM22 restricts SARS-CoV-2 replication by promoting proteasomal degradation of NSP8. *mBio*, *15*(2), e0232023. https://doi.org/10.1128/mbio.02320-23

Gao, W., Wang, L., Cui, W., Wang, H., Huang, G., Li, Z., Li, G., & Zhang, W. (2024). Deubiquitinase USP1 regulates sarbecovirus ORF6 protein function. *J Virol*, *98*(1), e0143723. https://doi.org/10.1128/jvi.01437-23

Gao, W., Wang, L., Ju, X., Zhao, S., Li, Z., Su, M., Xu, J., Wang, P., Ding, Q., & Lv, G. (2022). The deubiquitinase USP29 promotes SARS-CoV-2 virulence by preventing proteasome degradation of ORF9b. *Mbio*, *13*(3), e01300-01322.

[Record #31 is using a reference type undefined in this output style.]

Grice, G. L., & Nathan, J. A. (2016). The recognition of ubiquitinated proteins by the proteasome. *Cellular and molecular life sciences*, *73*, 3497-3506.

Guo, G., Gao, M., Gao, X., Zhu, B., Huang, J., Luo, K., Zhang, Y., Sun, J., Deng, M., & Lou, Z. (2021). SARS-CoV-2 non-structural protein 13 (nsp13) hijacks host deubiquitinase USP13 and counteracts host antiviral immune response. *Signal transduction and targeted therapy*, *6*(1), 119.

Hojyo, S., Uchida, M., Tanaka, K., Hasebe, R., Tanaka, Y., Murakami, M., & Hirano, T. (2020). How COVID-19 induces cytokine storm with high mortality. *Inflamm Regen*, *40*, 37. https://doi.org/10.1186/s41232-020-00146-3

Hu, B., Huang, S., & Yin, L. (2021). The cytokine storm and COVID-19. *J Med Virol*, *93*(1), 250-256. https://doi.org/10.1002/jmv.26232

Ju, X., Zhu, Y., Wang, Y., Li, J., Zhang, J., Gong, M., Ren, W., Li, S., Zhong, J., Zhang, L., Zhang, Q. C., Zhang, R., & Ding, Q. (2021). A novel cell culture system modeling the SARS-CoV-2 life cycle. *PLoS Pathog*, *17*(3), e1009439. https://doi.org/10.1371/journal.ppat.1009439

Kamimura, K., Kanefuji, T., Yokoo, T., Abe, H., Suda, T., Kobayashi, Y., Zhang, G., Aoyagi, Y., & Liu, D. (2014). Safety assessment of liver-targeted hydrodynamic gene delivery in dogs. *PLoS One*, *9*(9), e107203. https://doi.org/10.1371/journal.pone.0107203

Kim, J. G., Shin, H.-C., Seo, T., Nawale, L., Han, G., Kim, B. Y., Kim, S. J., & Cha-Molstad, H. (2021). Signaling pathways regulated by UBR box-containing E3 ligases. *International journal of molecular sciences*, *22*(15), 8323.

Klima, M., Khalili Yazdi, A., Li, F., Chau, I., Hajian, T., Bolotokova, A., Kaniskan, H. Ü., Han, Y., Wang, K., & Li, D. (2022). Crystal structure of SARS-CoV-2 nsp10–nsp16 in complex with small molecule inhibitors, SS148 and WZ16. *Protein Science*, *31*(9), e4395.

Li, Z., Hao, P., Zhao, Z., Gao, W., Huan, C., Li, L., Chen, X., Wang, H., Jin, N., & Luo, Z.-Q. (2023). The E3 ligase RNF5 restricts SARS-CoV-2 replication by targeting its envelope protein for degradation. *Signal Transduction and Targeted Therapy*, *8*(1), 53.

Liang, X., Xiao, J., Li, X., Liu, Y., Lu, Y., Wen, Y., Li, Z., Che, X., Ma, Y., & Zhang, X. (2022). A C-terminal glutamine recognition mechanism revealed by E3 ligase TRIM7 structures. *Nature Chemical Biology*, *18*(11), 1214-1223.

Lin, S., Chen, H., Ye, F., Chen, Z., Yang, F., Zheng, Y., Cao, Y., Qiao, J., Yang, S., & Lu, G. (2020). Crystal structure of SARS-CoV-2 nsp10/nsp16 2′-O-methylase and its implication on antiviral drug design. *Signal transduction and targeted therapy*, *5*(1), 131.

Lugari, A., Betzi, S., Decroly, E., Bonnaud, E., Hermant, A., Guillemot, J.-C., Debarnot, C., Borg, J.-P., Bouvet, M., & Canard, B. (2010). Molecular mapping of the RNA Cap 2′-O-methyltransferase activation interface between severe acute respiratory syndrome coronavirus nsp10 and nsp16. *Journal of Biological Chemistry*, *285*(43), 33230-33241.

Mahajan, S., Sharma, G. K., Bora, K., & Pattnaik, B. (2021). Identification of novel interactions between host and non-structural protein 2C of foot-and-mouth disease virus. *J Gen Virol*, *102*(3). https://doi.org/10.1099/jgv.0.001577

Maimaitiyiming, Y., Yang, T., Wang, Q. Q., Feng, Y., Chen, Z., Björklund, M., Wang, F., Hu, C., Hsu, C.-H., & Naranmandura, H. (2022). Heat treatment promotes ubiquitin-mediated proteolysis of SARS-CoV-2 RNA polymerase and decreases viral load. *Research*.

Makaremi, S., Asgarzadeh, A., Kianfar, H., Mohammadnia, A., Asghariazar, V., & Safarzadeh, E. (2022). The role of IL-1 family of cytokines and receptors in pathogenesis of COVID-19.

Inflamm Res, *71*(7-8), 923-947. https://doi.org/10.1007/s00011-022-01596-w

McClellan, A. J., Laugesen, S. H., & Ellgaard, L. (2019). Cellular functions and molecular mechanisms of non-lysine ubiquitination. *Open Biology*, *9*(9), 190147.

Melo-Filho, C. C., Bobrowski, T., Martin, H.-J., Sessions, Z., Popov, K. I., Moorman, N. J., Baric, R. S., Muratov, E. N., & Tropsha, A. (2022). Conserved coronavirus proteins as targets of broad-spectrum antivirals. *Antiviral Research*, *204*, 105360.

Muñoz-Escobar, J., Matta-Camacho, E., Kozlov, G., & Gehring, K. (2015). The MLLE domain of the ubiquitin ligase UBR5 binds to its catalytic domain to regulate substrate binding. *Journal of Biological Chemistry*, *290*(37), 22841-22850.

Nathan, J. A., Sengupta, S., Wood, S. A., Admon, A., Markson, G., Sanderson, C., & Lehner, P. J. (2008). The ubiquitin E3 ligase MARCH7 is differentially regulated by the deubiquitylating enzymes USP7 and USP9X. *Traffic*, *9*(7), 1130-1145.

Park, G. J., Osinski, A., Hernandez, G., Eitson, J. L., Majumdar, A., Tonelli, M., Henzler-Wildman, K., Pawłowski, K., Chen, Z., & Li, Y. (2022). The mechanism of RNA capping by SARS-CoV-2. *Nature*, *609*(7928), 793-800.

Qiao, X., Liu, Y., Prada, M. L., Mohan, A. K., Gupta, A., Jaiswal, A., Sharma, M., Merisaari, J., Haikala, H. M., & Talvinen, K. (2020). UBR5 is coamplified with MYC in breast tumors and encodes an ubiquitin ligase that limits MYC-dependent apoptosis. *Cancer research*, *80*(7), 1414-1427.

Raper, S. E., Chirmule, N., Lee, F. S., Wivel, N. A., Bagg, A., Gao, G. P., Wilson, J. M., & Batshaw, M. L. (2003). Fatal systemic inflammatory response syndrome in a ornithine transcarbamylase deficient patient following adenoviral gene transfer. *Mol Genet Metab*, *80*(1-2), 148-158. https://doi.org/10.1016/j.ymgme.2003.08.016

Rosas-Lemus, M., Minasov, G., Shuvalova, L., Inniss, N. L., Kiryukhina, O., Brunzelle, J., & Satchell, K. J. (2020). High-resolution structures of the SARS-CoV-2 2′-O-methyltransferase reveal strategies for structure-based inhibitor design. *Science signaling*, *13*(651), eabe1202.

Russ, A., Wittmann, S., Tsukamoto, Y., Herrmann, A., Deutschmann, J., Lagisquet, J., Ensser, A., Kato, H., & Gramberg, T. (2022). Nsp16 shields SARS–CoV-2 from efficient MDA5 sensing and IFIT1-mediated restriction. *EMBO reports*, *23*(12), e55648.

Shearer, R. F., Frikstad, K.-A. M., McKenna, J., McCloy, R. A., Deng, N., Burgess, A., Stokke, T., Patzke, S., & Saunders, D. N. (2018). The E3 ubiquitin ligase UBR5 regulates centriolar satellite stability and primary cilia. *Molecular biology of the cell*, *29*(13), 1542-1554.

Song, P., Li, W., Xie, J., Hou, Y., & You, C. (2020). Cytokine storm induced by SARS-CoV-2. *Clin Chim Acta*, *509*, 280-287. https://doi.org/10.1016/j.cca.2020.06.017

Suda, T., Yokoo, T., Kanefuji, T., Kamimura, K., Zhang, G., & Liu, D. (2023). Hydrodynamic Delivery: Characteristics, Applications, and Technological Advances. *Pharmaceutics*, *15*(4). https://doi.org/10.3390/pharmaceutics15041111

Wu, B., Song, M., Dong, Q., Xiang, G., Li, J., Ma, X., & Wei, F. (2022). UBR5 promotes tumor immune evasion through enhancing IFN-γ-induced PDL1 transcription in triple negative breast cancer. *Theranostics*, *12*(11), 5086.

Xiang, G., Wang, S., Chen, L., Song, M., Song, X., Wang, H., Zhou, P., Ma, X., & Yu, J. (2022). UBR5 targets tumor suppressor CDC73 proteolytically to promote aggressive breast cancer. *Cell Death & Disease*, *13*(5), 451.

Xu, G., Wu, Y., Xiao, T., Qi, F., Fan, L., Zhang, S., Zhou, J., He, Y., Gao, X., & Zeng, H. (2022).

743 Multiomics approach reveals the ubiquitination-specific processes hijacked by
744 SARS-CoV-2. *Signal Transduction and Targeted Therapy*, *7*(1), 312.
745 Zhang, H., Zheng, H., Zhu, J., Dong, Q., Wang, J., Fan, H., Chen, Y., Zhang, X., Han, X., & Li, Q.
746 (2021). Ubiquitin-modified proteome of SARS-CoV-2-infected host cells reveals insights
747 into virus–host interaction and pathogenesis. *Journal of Proteome Research*, *20*(5),
748 2224-2239.
749 Zhang, J., Cruz-Cosme, R., Zhuang, M.-W., Liu, D., Liu, Y., Teng, S., Wang, P.-H., & Tang, Q. (2020).
750 A systemic and molecular study of subcellular localization of SARS-CoV-2 proteins.
751 *Signal transduction and targeted therapy*, *5*(1), 269.
752 Zhang, L., Hao, P., Chen, X., Lv, S., Gao, W., Li, C., Li, Z., & Zhang, W. (2024). CRL4B E3 ligase
753 recruited by PRPF19 inhibits SARS-CoV-2 infection by targeting ORF6 for
754 ubiquitin-dependent degradation. *mBio*, *15*(2), e0307123.
755 https://doi.org/10.1128/mbio.03071-23
756 Zhang, L., Wang, H., Tian, L., & Li, H. (2016). Expression of USP7 and MARCH7 is correlated with
757 poor prognosis in epithelial ovarian cancer. *The Tohoku journal of experimental medicine*,
758 *239*(3), 165-175.
759 Zhang, X., Yang, Z., Pan, T., Sun, Q., Chen, Q., Wang, P. H., Li, X., & Kuang, E. (2023). SARS-CoV-2
760 Nsp8 suppresses MDA5 antiviral immune responses by impairing TRIM4-mediated
761 K63-linked polyubiquitination. *PLoS Pathog*, *19*(11), e1011792.
762 https://doi.org/10.1371/journal.ppat.1011792
763 Zhao, K., Yang, Y., Zhang, G., Wang, C., Wang, D., Wu, M., & Mei, Y. (2018). Regulation of the
764 Mdm2–p53 pathway by the ubiquitin E3 ligase MARCH 7. *EMBO reports*, *19*(2), 305-319.
765 Zheng, C. (2021). The emerging roles of the MARCH ligases in antiviral innate immunity.
766 *International Journal of Biological Macromolecules*, *171*, 423-427.
767 Zhou, Y., Zheng, R., Liu, D., Liu, S., Disoma, C., Li, S., Liao, Y., Chen, Z., Du, A., & Dong, Z. (2022).
768 UBR5 Acts as an Antiviral Host Factor against MERS-CoV via Promoting Ubiquitination
769 and Degradation of ORF4b. *Journal of Virology*, *96*(17), e00741-00722.
770 Züst, R., Cervantes-Barragan, L., Habjan, M., Maier, R., Neuman, B. W., Ziebuhr, J., Szretter, K. J.,
771 Baker, S. C., Barchet, W., & Diamond, M. S. (2011). Ribose 2′-O-methylation provides a
772 molecular signature for the distinction of self and non-self mRNA dependent on the RNA
773 sensor Mda5. *Nature immunology*, *12*(2), 137-143.
774

775

776 **Figure legends**

777 **Figure 1. The non-structural protein nsp16 of SARS-CoV-2 was identified that can**
778 **be degraded through the proteasome pathway.**

779 A. The non-structural proteins nsp8, nsp11 and nsp16 could be restored by the
780 proteasome inhibitor MG132. HEK293T cells in 12-well plates were transfected with the
781 plasmids of 16 nonstructural proteins (nsp1-16) encoded by SARS-CoV-2. Thirty-six hours
782 later, the cells were treated with MG132 (10 μM) or DMSO for 12 h before collection. The
783 protein level was detected by Immunoblotting (IB). Quantification of nsp protein levels
784 relative to the control protein is shown. Data are representative of three independent
785 experiments and shown as average ±SD (n = 3). Significance was determined by a
786 two-tailed t-test: *P < 0.05; **P < 0.01; ***P < 0.001.

787 B. Proteasomal inhibitors but no other inhibitors stabilized nsp16 protein. HEK293T cells
788 transfected with the nsp16-Flag expression vector were treated with dimethyl sulfoxide
789 (DMSO), MG132 (10 μM), Bortezomib (10 μM), Carfilzomib (10 μM), Bafilomycin A1 (5
790 μM), Vinblastine (2.5 μM), or NH_4CL (2.5 μM) for 12 h prior to harvest. The cell lysates
791 were analyzed by anti-Flag antibody.

792 (C-D). The half-life of nsp16 was prolonged by the proteasome inhibitor MG132. C.
793 HEK293T cells were transfected with the nsp16-Flag-expressing plasmids. 12 hours later,
794 the cells were treated with DMSO or MG132 (10 μM) for 12 h, then 50 μg/mL
795 cycloheximide (CHX) was added. Cells were harvested at the indicated times to detect the
796 level of viral protein by anti-Flag antibody. D. Quantification of nsp16 protein levels relative
797 to tubulin at different time points is shown. The half-life of the nsp16 protein was
798 determined based on protein quantification using Image J, combined with the protein
799 half-life formula for calculation. Results are shown as mean ± SD (n = 3 independent
800 experiments). ***, P < 0.001 by by a two-tailed t-test.

801 E. Samples were prepared for mass spectrometry, and nsp16 interacting proteins were
802 obtained by immunoprecipitation (IP) (created with BioRender.com and the agreement no.
803 is LC27PCBEOF). The plasmids were transfected into HEK293T cells for 48 h. Treat cells

804 with or without MG132 (10 μM) for 12 h prior to harvest. The whole-cell lysates were
805 incubated with protein G agarose beads conjugated with anti-Flag antibodies and used for
806 IB with anti-Flag antibodies to detect the nsp16 protein. Samples enriched for proteins
807 were analyzed by mass spectrometry.

808 **Figure 1—figure supplement 1. Analysis of mass spectrometry results.**

809 A. The DAVID bioinformatics website (https://david.ncifcrf.gov/tools.jsp) was used for
810 KEGG pathway analysis and GO analysis of the differential proteins bound by nsp16
811 protein after treating with or without MG132. The bubble plots or circle diagram depict the
812 results of the analysis separately. In bubble plots, a change from yellow to purple indicates
813 a decreased p-value, while the size of the circles indicates the number of enriched genes.
814 In the circle plot, depicting the BP (Biological process) analysis in the GO term, the length
815 of the purple rectangle indicates the number of genes included in the term. The length of
816 the green rectangle indicates the number of overlapping genes between the genes
817 included in the term and the genes entered in the gene enrichment analysis, a change
818 from deep to shallow of purple indicates a decreased p-value (created with chiplot.com).
819 B. Schematic representation of proteins degraded by the proteasome pathway, as well as
820 proteins associated with the proteasome in the MS enrichment analysis are
821 shown (created with BioRender.com and the agreement no. is VO27O5XHHC).

822 **Figure 2. MARCHF7 and UBR5 were identified as E3 ubiquitin ligases involves in**
823 **nsp16 protein degradation.**

824 A. Knockdown of MARCHF7 or UBR5 resulted in nsp16 restoration. HEK293T cells were
825 transfected with siRNA of E3 ligase candidates for 24 h, followed by co-incubation with the
826 nsp16-Flag-expressing plasmids for 48 h, treated with MG132 (10 μM) for 16h before
827 harvesting, lysed, and subjected to IB assay using anti-Flag antibody. RT-qPCR was
828 conducted to determine the mRNA expression levels of E3 ligase candidates. The si-RNA
829 targeting regions for the candidate E3 ubiquitin ligase proteins and the targeted regions
830 for RT-qPCR are shown in Appendix-figure S1A. Data are representative of three
831 independent experiments and shown as average ± SD (n = 3). Significance was

832 determined by a two-tailed t-test: ***P < 0.001.

833 B. RNA levels of UBR5 or MARCHF7 from HEK293T cells infected with lentivirus
834 containing control or shRNA targeting UBR5 or MARCHF7 for 48 h and screened with
835 antibiotics for 48 h. Knockdown cell lines were transfected with plasmids expressing
836 nsp16-Flag, collected at the indicated times, and the protein levels of nsp16, MARCHF7,
837 and UBR5 were detected by IB.C. MARCHF7 and UBR5 acted separately and did not
838 depend on each other. HEK293T cells stably expressing UBR5 shRNA or MARCHF7
839 shRNA were transfected with siRNA of MARCHF7 or UBR5 for 24 h, respectively, followed
840 by co-incubation with the nsp16-Flag-expressing plasmids for 48 h. The protein levels and
841 the RNA levels of nsp16, UBR5 and MARCHF7 were measured by IB and RT-qPCR,
842 respectively.

843 (D-E). In HEK293T cells stably expressing UBR5 shRNA or MARCHF7 shRNA, nsp16
844 was degraded by overexpressed UBR5 or MARCHF7, respectively, whereas the mutant
845 failed to degrade nsp16. The cell lysates were analyzed by anti-Flag antibody.

846 **Figure 2—figure supplement 1. MARCHF7 and UBR5 degrade nsp16 independently.**

847 (A-B). UBR5 siRNA was transfected into shMARCHF7 cells to knock down UBR5. After 24
848 hours, MARCHF7 and nsp16 expression vectors were co-transfected, and the cells were
849 harvested 72 hours later. The levels of nsp16 were characterized by IB with anti-Flag
850 antibody. Whether MARCHF7 was dependent on UBR5 to degrade of nsp16 was
851 determined by further transfection of MARCHF7 siRNA into shUBR5 cells, followed by
852 co-transfection of UBR5 and nsp16 expression vectors 24 h later. The other operations
853 are the same as above. Data are representative of three independent experiments and
854 shown as average ±SD (n = 3). Significance was determined by a two-tailed t-test. *P >
855 0.05; **P < 0.01; ***P < 0.001.

856 **Figure 3. MARCHF7 or UBR5 catalyze the formation of K-27 type or K-48 type**
857 **ubiquitin chains of nsp16 respectively.**

858 A. Nsp16 can be ubiquitinated. HEK293T cells co-transfected with ubiquitin-Myc and
859 nsp16-Flag or transfected with nsp16-Flag alone. The cells were treated with MG132 for

860 12 h before collection. The whole-cell lysates were incubated with anti-Flag beads and
861 used for IB with anti-Myc or anti-Flag antibodies to detect the polyubiquitination chain of
862 nsp16.
863 B. Assess the endogenous ubiquitination level of nsp16 protein. Cells were transfected
864 with nsp16-Flag or an empty vector, and collected 48 hours later. Prior to harvesting, cells
865 were treated with MG132 for 16 hours. Co-IP experiments were then performed to
866 analyze the endogenous ubiquitination level of nsp16.
867 C. The level of ubiquitination of nsp16 decreased with decreasing the protein levels of
868 MARCHF7 or UBR5. E3 was knocked down by transfection with siRNA targeting UBR5 or
869 MARCHF7, and 24 h later ubiquitin-Myc and nsp16-HA were co-transfected or nsp16-HA
870 alone. Cells were treated with MG132 for 16 h before collection. Whole cell lysates were
871 incubated with anti-HA beads, and polyubiquitinated chains of nsp16 were detected by IB
872 with anti-Myc or anti-HA antibodies.
873 D. Nsp16 can be modified by a variety of ubiquitin chains. HEK293T cells were
874 transfected with either nsp16-HA alone or together with plasmids encoding various
875 mutants of ubiquitin (K6 only, K11 only, K27 only, K29 only, K33 only, K48 only, K63 only).
876 Thirty-six hours later, cells were treated with MG132 for 12 h. Cell lysates were then
877 subjected to immunoprecipitation, followed by IB to analysis.
878 (E-F) MARCHF7 or UBR5 causes nsp16 to be modified by the K27 type or K48 type
879 ubiquitin chain. 293T cell lines with or without MARCHF7 or UBR5 knockdown were
880 co-transfected with plasmids encoding ubiquitin-WT or various mutants of ubiquitin (K6
881 only, K11 only, K27 only, K29 only, K33 only, K48 only, K63 only). The other experimental
882 methods were the same as C.
883 **Figure 4. MARCHF7 and UBR5 directly interact with nsp16 respectively.**
884 (A-B). The binding of MARCHF7 or UBR5 to nsp16 was not mutually dependent. The
885 binding of nsp16 to UBR5 or MARCHF7 was identified by co-immunoprecipitation in
886 HEK293T cells transfected siMARCHF7 or siUBR5, respectively. The immunoprecipitates
887 and input were analyzed by IB. The knockdown efficiency was detected by RT-qPCR and
888 IB.

889 (C-D). MARCHF7 or UBR5 co-localized with nsp16 in the endoplasmic reticulum. Hela
890 cells were co-transfected with YFP-nsp16(yellow) and CFP-UBR5(cyan) or
891 CFP-MARCHF7(cyan). The organelles were labeled with antibodies against marker
892 proteins of endoplasmic reticulum, Golgi apparatus and mitochondria respectively(red).
893 The cells were analyzed by confocal microscopy (C). Scale bars, 20 um. The ratio of
894 colocalization was quantified by measuring the fluorescence intensities using Image J (D).

895 **Figure 4—figure supplement 1. Interaction of MARCHF7 or UBR5 with nsp16.**

896 A. HEK293T cells were transfected with either nsp16-Flag alone or together with
897 MARCHF7-Myc. Thirty-six hours after transfection, the cells were treated with MG132 (10
898 μM) for 12 h. Cell lysates were subjected to immunoprecipitation with anti-Flag antibody.
899 Using IB to analyze the precipitates and input.

900 B. HEK293T cells were transfected with nsp16-Flag. Cell lysates were subjected to
901 immunoprecipitation with anti-UBR5 or IgG antibody.

902 (C-D). Hela cells were co-transfected with YFP-nsp16 and CFP-UBR5 or CFP-MARCHF7.
903 A representative image of YFP-nsp16 (yellow) and ECFP-MARCHF7 (cyan) or
904 ECFP-UBR5 (cyan) expressing cells before and after photobleaching the acceptor
905 fluorophore, YFP. The region chosen for photobleaching is marked (white open box), Bars,
906 10um. The quantization of fluorescence brightness was analyzed by Image J. Data are
907 representative of three independent experiments and shown as average ±SD (n = 3).
908 Significance was determined by a two-tailed t-test. *P > 0.05; **P < 0.01; ***P < 0.001.

909 E. HeLa cells transfected with nsp16-Flag were analyzed by confocal microscopy. The
910 Flag-tagged nsp16 labeled with anti-Flag antibody (red). MARCHF7 or UBR5 were
911 labeled with endogenous antibodies (green). Cell nuclei were stained using DAPI (blue).
912 Representative images were shown. Scale bars, 20 um. The ratio of colocalization was
913 quantified by measuring the fluorescence intensities using Image J.

914 F. nsp16 was stably transfected into HEK293T cells. The cells were analyzed by confocal
915 microscopy. The other operations are the same as above.

916 **Figure 4—figure supplement 2. Domains in which MARCHF7 or UBR5 functions.**

917 A. The schematic represents UBR5 WT or mutants used in the study.

918 B. The HECT domain of UBR5 is required for nsp16 degradation. After co-transfection
919 with UBR5 WT or mutants and nsp16-HA, cells were harvested 48 hours later, and cell
920 lysates were examined by IB.

921 C. The HECT domain of UBR5 affects K48-type ubiquitin chain of nsp16.HEK293T cells
922 were transfected with the assigned plasmids. After 36 hours, cells were treated with 10 μM
923 MG132 for 12 hours, harvested, and cell lysates were incubated with protein G agarose
924 beads conjugated with anti-HA antibodies. Cell lysates and precipitated samples were
925 analyzed by IB.

926 D. The schematic represents wild-type and truncated forms of MARCHF7 used in the
927 study. E. Only MARCHF7 wild-type degraded nsp16.

928 F. The N-terminal region of MARCHF7 interacted with nsp16, and only the wild type could
929 catalyze the K27-type ubiquitin chain of nsp16.

930 **Figure 5. Knockdown of MARCHF7 or UBR5 promotes viral replication.**

931 A. The virus-encoded nsp16 protein interacts with endogenous MARCHF7 and UBR5 and
932 undergoes ubiquitination modification. In 293T-ACE2 cells, with or without Wuhan strain
933 infection (MOI: 0.01), the medium was changed 2 hours post-infection, and cells were
934 harvested 48 hours later, with MG132 treatment added 16 hours before harvesting. nsp16
935 protein was enriched using Protein-G beads coupled with the nsp16 antibody, and
936 interactions and ubiquitination were analyzed by immunoblotting (IB) with endogenous
937 antibodies against MARCHF7, UBR5, and ubiquitination.

938 (B-I). MARCHF7 and UBR5 were knocked down by siRNA in Caco2 cells. 24 h after
939 transfection, the cells were infected with Wuhan strain (MOI:0.01) (C-E) or Omicron BA.1
940 strain (MOI: 0.001) (F-H), respectively. 2 h post infection, the supernatant was discarded,
941 and the cells were cultured in DMEM containing 3% fetal bovine serum for 48 h. The
942 mRNA levels of SARS-CoV-2 *M* and *E* genes in the cells (C, F) and *E* genes in
943 supernatant (D, G) were detected by RT-qPCR and the viral titers in supernatant (E, H)
944 were measured. The N protein levels of Wuhan or Omicron viruses were detected by IB (I).
945 Knock-down efficiencies of MARCHF7 and UBR5 were detected by RT-qPCR or IB (B, I).

946 Data are representative of three independent experiments and shown as average ±SD (n
947 = 3). Significance was determined by one-way ANOVA, followed by a Tukey multiple
948 comparisons posttest: *P < 0.05; **P < 0.01; ***P < 0.001.

949 **Figure 5—figure supplement 1. Effect of MARCHF7 or UBR5 on SARS-CoV-2 trVLP.**

950 (A-B). Knocking down MARCHF7 or UBR5 enhances SARS-CoV-2 trVLP infectivity.
951 MARCHF7 or UBR5 was knocked down by siRNA in Caco2 cells with stable expression of
952 SARS-CoV-2 N protein. Twenty-four hours later, cells were infected with SARS-CoV-2
953 virus-like-particles (MOI:0.1), the medium was changed two hours after infection, and the
954 eGFP-positive cells were detected by flow cytometry 48 hours later (A). Protein content
955 was determined by RT-qPCR (B).

956 **Figure 6. Increased levels of nsp16 rescued viral inhibition by UBR5 or MARCHF7'**

957 (A-H) UBR5 or MARCHF7 was transfected in 293T cells stably overexpressed with ACE2,
958 and the increased doses of nsp16-Flag was transfected simultaneously. After 24 h, the
959 cells were infected with Wuhan strains. The mRNA levels of *M* and *E* genes of Wuhan
960 strain in the cells (A, D) and *E* gene in supernatant (B, E) were detected by RT-qPCR, as
961 well as the detection of viral titers in supernatant (C, F). The N protein of the virus and the
962 overexpression efficiency was detected by IB (G, H). Data are representative of three
963 independent experiments and shown as average ±SD (n = 3). Significance was
964 determined by one-way ANOVA, followed by a Tukey multiple comparisons posttest. P >
965 0.05; **P < 0.01; ***P < 0.001. Figure 6—figure supplement 1 shows data related to
966 infection with Omicron BA.1.

967 **Figure 6—figure supplement 1. Effect of MARCHF7 or UBR5 on Omicron BA.1**
968 **infectivity.**

969 (A-H). Showing data related to infection with Omicron BA.1. The experimental procedure
970 was the same as Figure 6. Data are representative of three independent experiments and
971 shown as average ±SD (n = 3). Significance was determined by one-way ANOVA,
972 followed by a Tukey multiple comparisons posttest. P > 0.05; **P < 0.01; ***P < 0.001.

973 **Figure 6—figure supplement 2. The enzyme activity-deficient mutants do not exhibit**

974 **antiviral activity, and overexpression of nsp16 does not promote viral replication.**
975 (A-H) In 293T-ACE2 cells, the RING domain deletion mutant of MARCHF7
976 (MARCHF7-1-542) or the HECT domain inactivated mutant of UBR5 (UBR5-△HECT)
977 were transfected, along with a gradient of nsp16-Flag overexpression. The cells were
978 infected with the Wuhan strain (MOI: 0.01), medium was changed 2 hours post-infection,
979 and cells and supernatants were collected 48 hours after infection.
980 **Figure 6—figure supplement 3. MARCHF7 or UBR5 have effects on mutant of nsp16**
981 **in different subtypes of SARS-CoV-2.**
982 A. This diagram shows the mutation of nsp16 in different virus subtypes. The amino acids
983 sequences of different SARS-CoV-2 strains were obtained from NCBI, and the amino
984 acids sequences of nsp16 of different strains were compared by DNAMAN software.
985 B. Nsp16 mutants can still be regulated by MG132. The mutated nsp16 plasmids were
986 transfected into HEK293T cells. After 36 hours of culture, cells were treated with 10 μm
987 MG132 or DMSO, harvested 12 hours later, and cell lysates were examined by IB.
988 C. MARCHF7 or UBR5 can degrade nsp16 mutants. After transfecting MARCHF7 or
989 UBR5 siRNA and the mutated nsp16 plasmids, the cells were harvested 48 h later. The
990 cell lysates were detected by IB.
991 **Figure 6—figure supplement 4. The expression level of MARCHF7 was negatively**
992 **correlated with the viral titer, while the expression level of UBR5 was increased at**
993 **low titer and decreased at high titer.**
994 (A-C). The protein and mRNA levels of MARCHF7 or UBR5 upon infection with different
995 titers. Endogenous MARCHF7 and UBR5 RNA levels were detected by RT-qPCR 48
996 hours after infection with different titers of Wuhan strain (MOI:0, 0.0001, 0.001, 0.01) or
997 omicron BA.1 strain (MOI:0, 0.0001, 0.001). Protein levels were examined by IB.
998 D. The expression level of UBR5 was negatively correlated with the severity of the
999 disease but MARCHF7 expression levels were not. PBMC cells were extracted from
1000 common, severe and critical COVID-19 patients. RT-qPCR was used to detect the mRNA
1001 level of UBR5 or MARCHF7 in patients. Significance was determined by one-way ANOVA,

1002 followed by a Tukey multiple comparisons posttest. ns, P > 0.05; **P < 0.01; ***P < 0.001.

1003 **Figure 7. In a mouse infection model, overexpression of MARCHF7 or UBR5 exerted**
1004 **inhibitory effects on virus.**

1005 (A-G) BLAB/C mice were injected with the corresponding plasmids at 40ug/500ul via the
1006 high-pressure tail vein, followed by nasal inoculation with 50μl SARS-CoV-2 virus at a
1007 dosage of $10^{5.5}$ TCID50/mL (created with BioRender.com and the agreement no. is
1008 FO27O5X39A). IB was used to detect the expression of MARCHF7 or UBR5 in the lung
1009 tissues (B). Viral RNA loads in mouse lung tissues were detected by measuring the mRNA
1010 levels of the E genes by RT-qPCR (C). Lung tissue was collected, homogenized, and the
1011 residue was removed by centrifugation to collect the supernatant. The viral titer was then
1012 measured using the TCID50 method (D). Mouse body weight was monitored during the
1013 experimental period (E). Representative images of H&E staining of lungs of mice with
1014 different treatments. Magnification, ×40. Bars, 20 μm (F). The staining of viral N proteins.
1015 Magnification, ×63. Bars, 20 μm. n =3 in each group (G). RT-qPCR was used to measure
1016 the expression of cytokines and chemokines in the spleens of mice in each group (H).
1017 Statistical significance was analyzed using a one-way analysis of variance with Tukey's
1018 multiple comparisons test. (NS, no significance, *p < 0.05, **p < 0.01, ***p < 0.001).

1019 **Figure 8. Schematic diagram of MARCHF7 and UBR5 ubiquitinate the SARS-CoV-2**
1020 **non-structural protein nsp16, leading to its degradation via the proteasomal**
1021 **pathway, thereby affecting viral replication (created with BioRender.com and the**
1022 **agreement no. is FM27O5ZS3U).**

1023

Figure 1

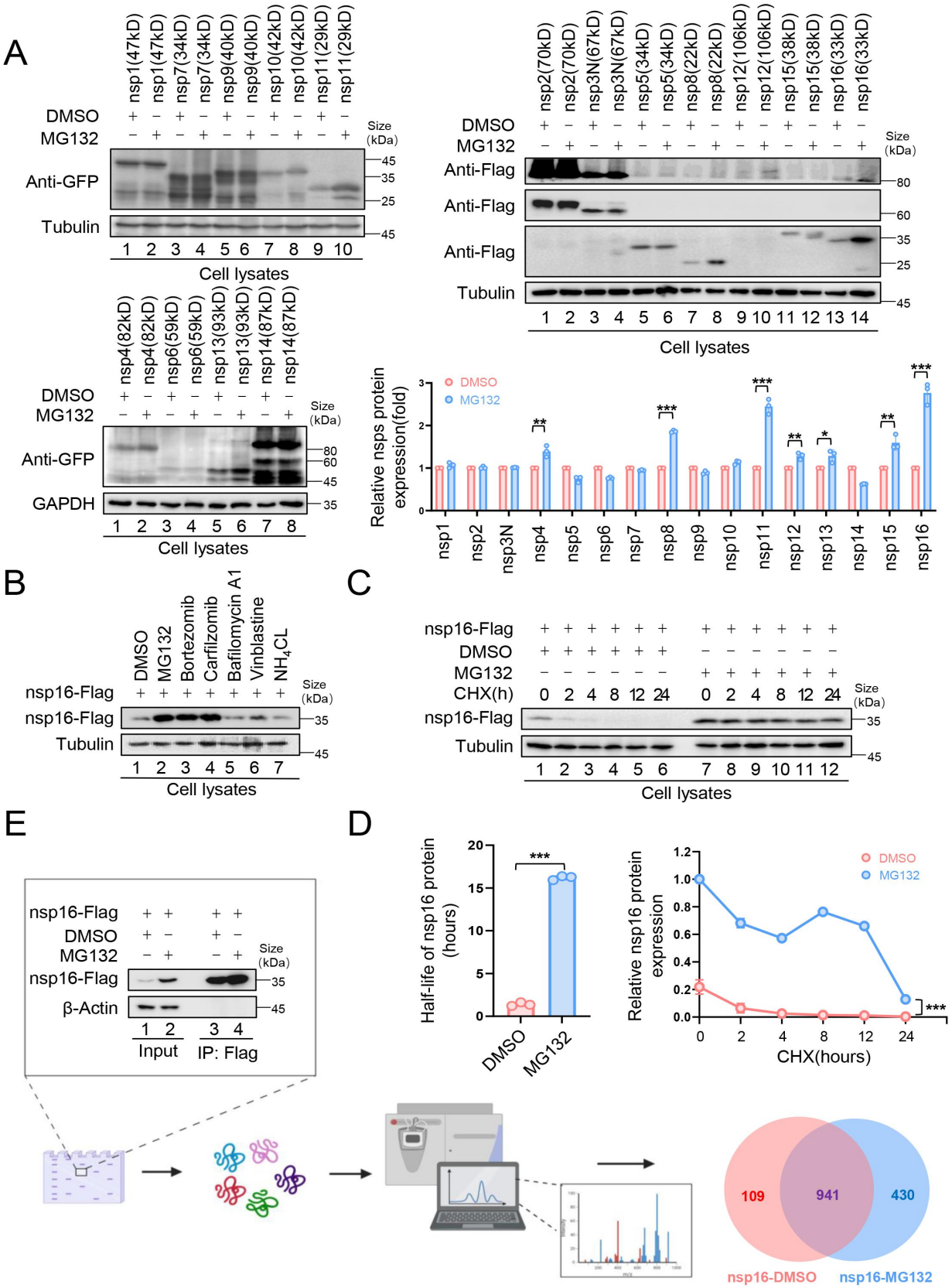
A
nsp1(47kD)
nsp7(34kD)
nsp9(40kD)
nsp10(42kD)
nsp11(29kD)
DMSO
MG132
Size (kDa)
Anti-GFP
Tubulin
Cell lysates
nsp2(70kD)
nsp3N(67kD)
nsp5(34kD)
nsp8(22kD)
nsp12(106kD)
nsp15(38kD)
nsp16(33kD)
Anti-Flag
nsp4(82kD)
nsp6(59kD)
nsp13(93kD)
nsp14(87kD)
GAPDH
Relative nsps protein expression(fold)
DMSO
MG132
B
DMSO
MG132
Bortezomib
Carfilzomib
Bafilomycin A1
Vinblastine
NH4CL
nsp16-Flag
C
CHX(h)
D
Half-life of nsp16 protein (hours)
Relative nsp16 protein expression
CHX(hours)
E
β-Actin
Input
IP: Flag
109
941
430
nsp16-DMSO
nsp16-MG132

Figure 1 supplement 1

A

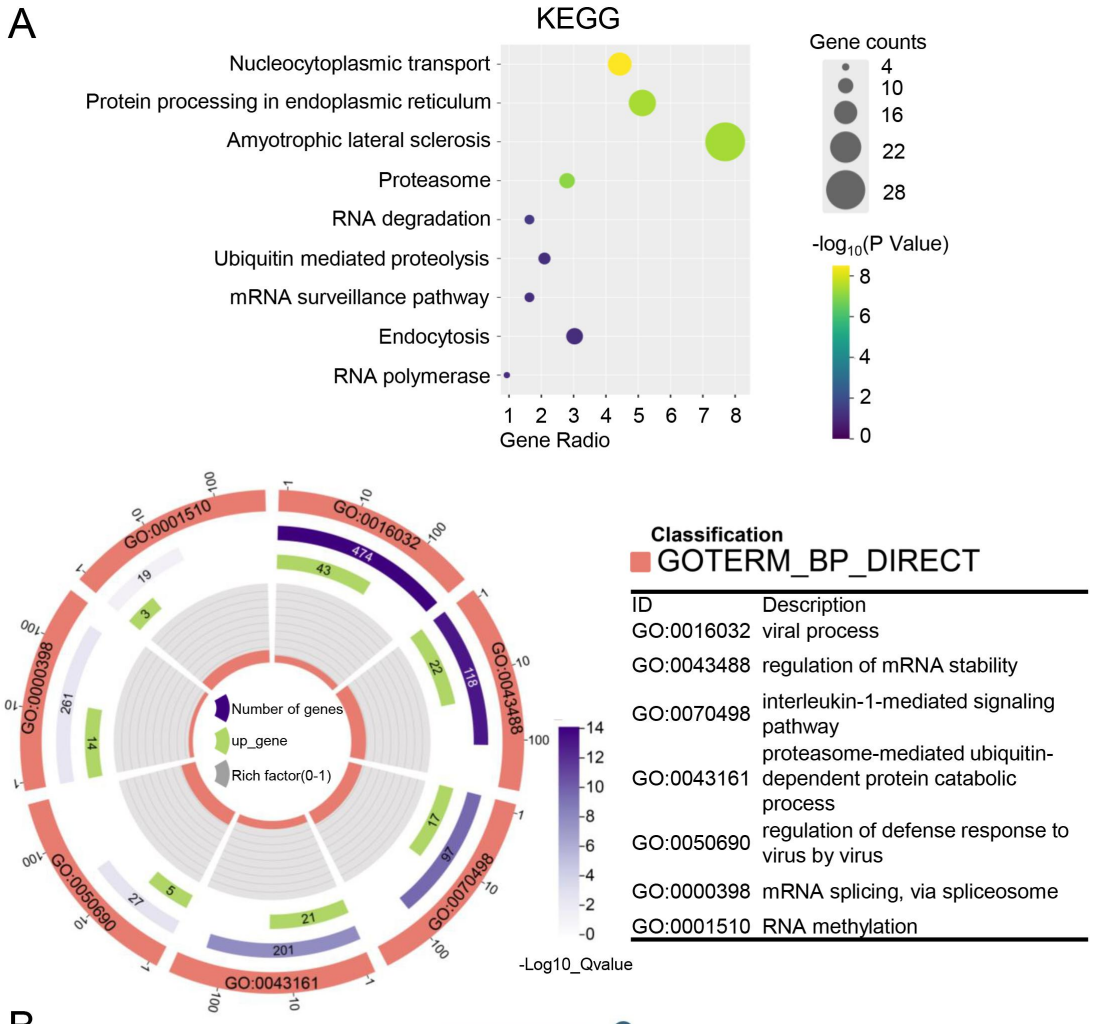

B

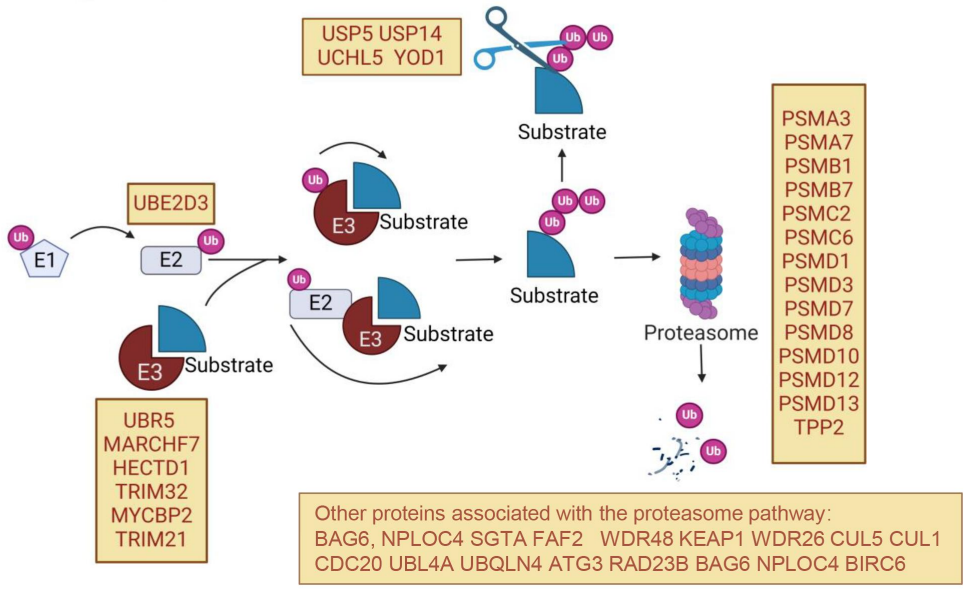

Figure 2

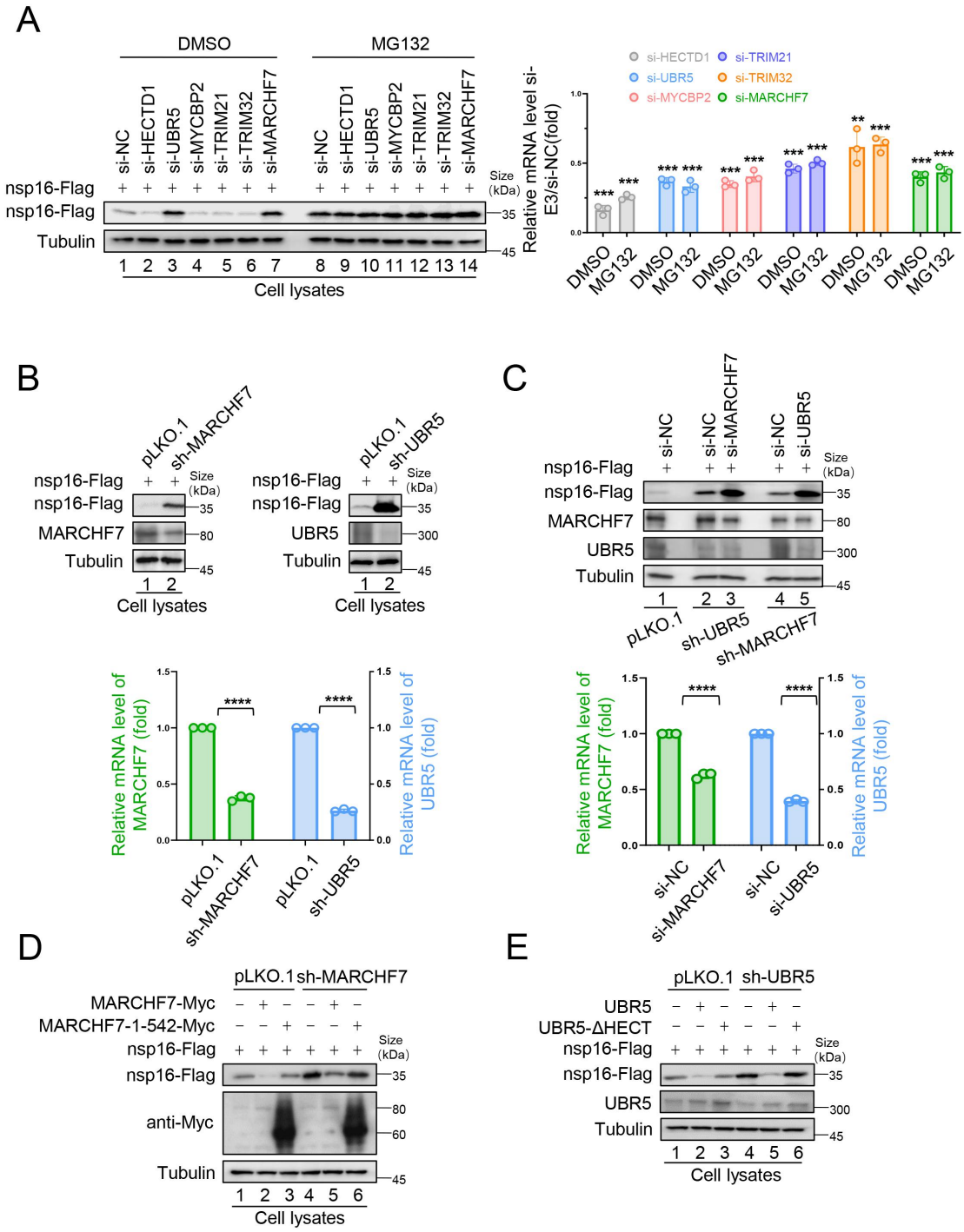
A
DMSO
MG132
si-NC
si-HECTD1
si-UBR5
si-MYCBP2
si-TRIM21
si-TRIM32
si-MARCHF7
nsp16-Flag
Tubulin
Size (kDa)
35
45
1 2 3 4 5 6 7 8 9 10 11 12 13 14
Cell lysates
Relative mRNA level si-E3/si-NC(fold)
si-HECTD1
si-UBR5
si-MYCBP2
si-TRIM21
si-TRIM32
si-MARCHF7
DMSO
MG132
B
pLKO.1
sh-MARCHF7
sh-UBR5
MARCHF7
UBR5
80
300
1 2
Cell lysates
Relative mRNA level of MARCHF7 (fold)
Relative mRNA level of UBR5 (fold)
****
C
si-NC
si-MARCHF7
si-UBR5
1 2 3 4 5
D
pLKO.1
sh-MARCHF7
MARCHF7-Myc
MARCHF7-1-542-Myc
anti-Myc
60
1 2 3 4 5 6
E
UBR5
UBR5-ΔHECT

Figure 2 supplement 1

A

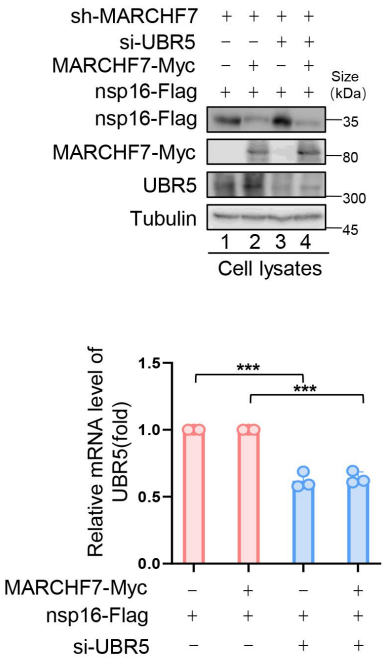

B

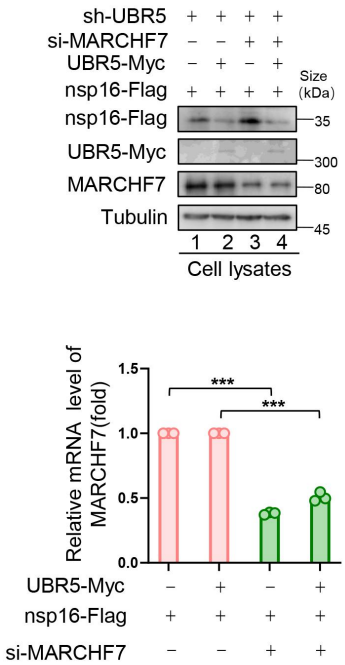

Figure 3

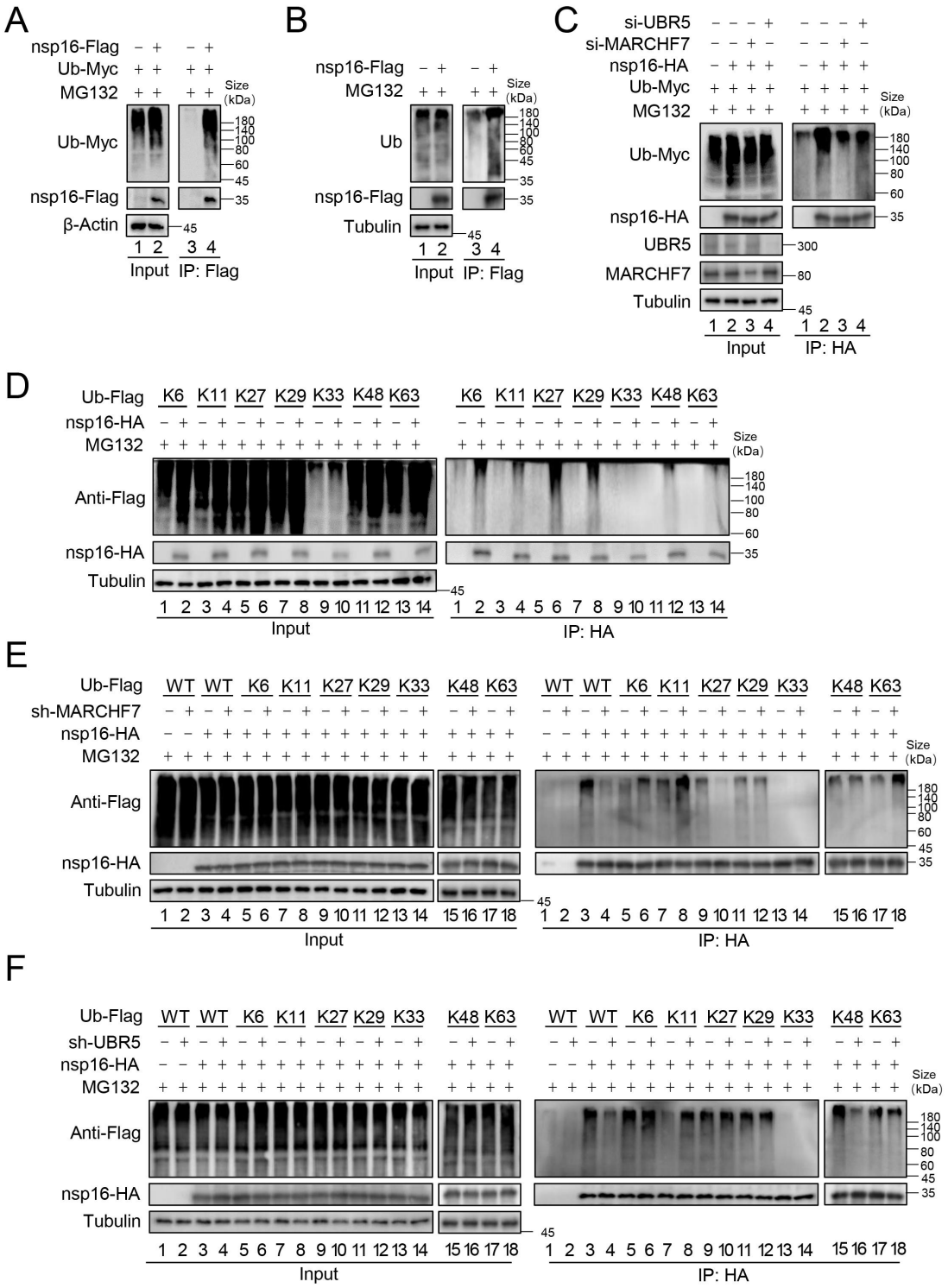
A
nsp16-Flag
Ub-Myc
MG132
Size (kDa)
Ub-Myc
nsp16-Flag
β-Actin
Input
IP: Flag
B
nsp16-Flag
MG132
Ub
nsp16-Flag
Tubulin
Input
IP: Flag
C
si-UBR5
si-MARCHF7
nsp16-HA
Ub-Myc
MG132
Ub-Myc
nsp16-HA
UBR5
MARCHF7
Tubulin
Input
IP: HA
D
Ub-Flag
K6 K11 K27 K29 K33 K48 K63
nsp16-HA
MG132
Anti-Flag
nsp16-HA
Tubulin
Input
IP: HA
E
Ub-Flag
WT WT K6 K11 K27 K29 K33 K48 K63
sh-MARCHF7
nsp16-HA
MG132
Anti-Flag
nsp16-HA
Tubulin
Input
IP: HA
F
Ub-Flag
WT WT K6 K11 K27 K29 K33 K48 K63
sh-UBR5
nsp16-HA
MG132
Anti-Flag
nsp16-HA
Tubulin
Input
IP: HA

Figure 4

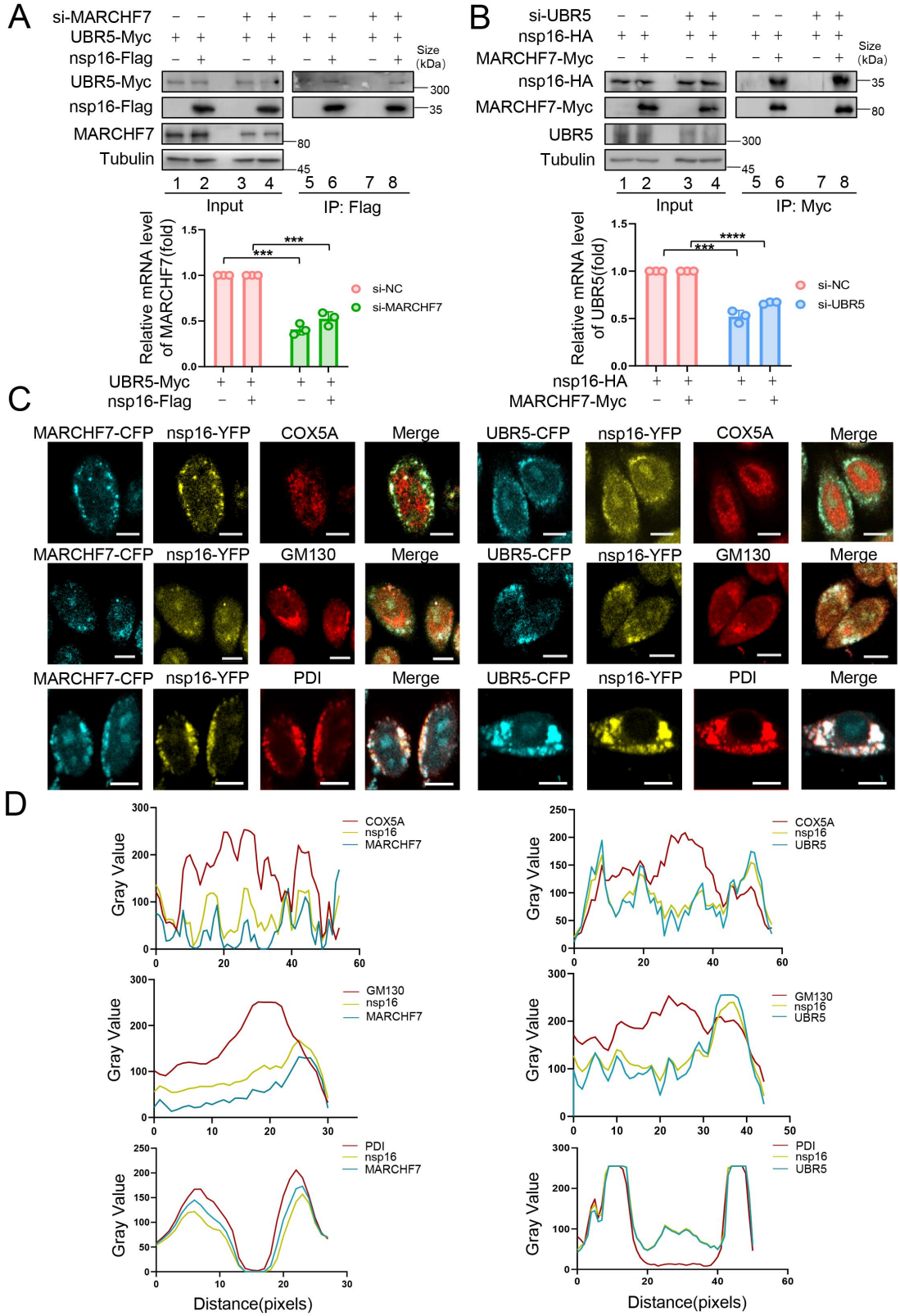
A
si-MARCHF7
UBR5-Myc
nsp16-Flag
UBR5-Myc
nsp16-Flag
MARCHF7
Tubulin
Size (kDa)
300
35
80
45
1 2 3 4 5 6 7 8
Input
IP: Flag
Relative mRNA level of MARCHF7(fold)
si-NC
si-MARCHF7
B
si-UBR5
nsp16-HA
MARCHF7-Myc
nsp16-HA
MARCHF7-Myc
UBR5
Tubulin
Input
IP: Myc
Relative mRNA level of UBR5(fold)
si-NC
si-UBR5
C
MARCHF7-CFP
nsp16-YFP
COX5A
GM130
PDI
Merge
UBR5-CFP
D
Gray Value
Distance(pixels)
COX5A
GM130
PDI
nsp16
MARCHF7
UBR5

Figure 4 supplement 1

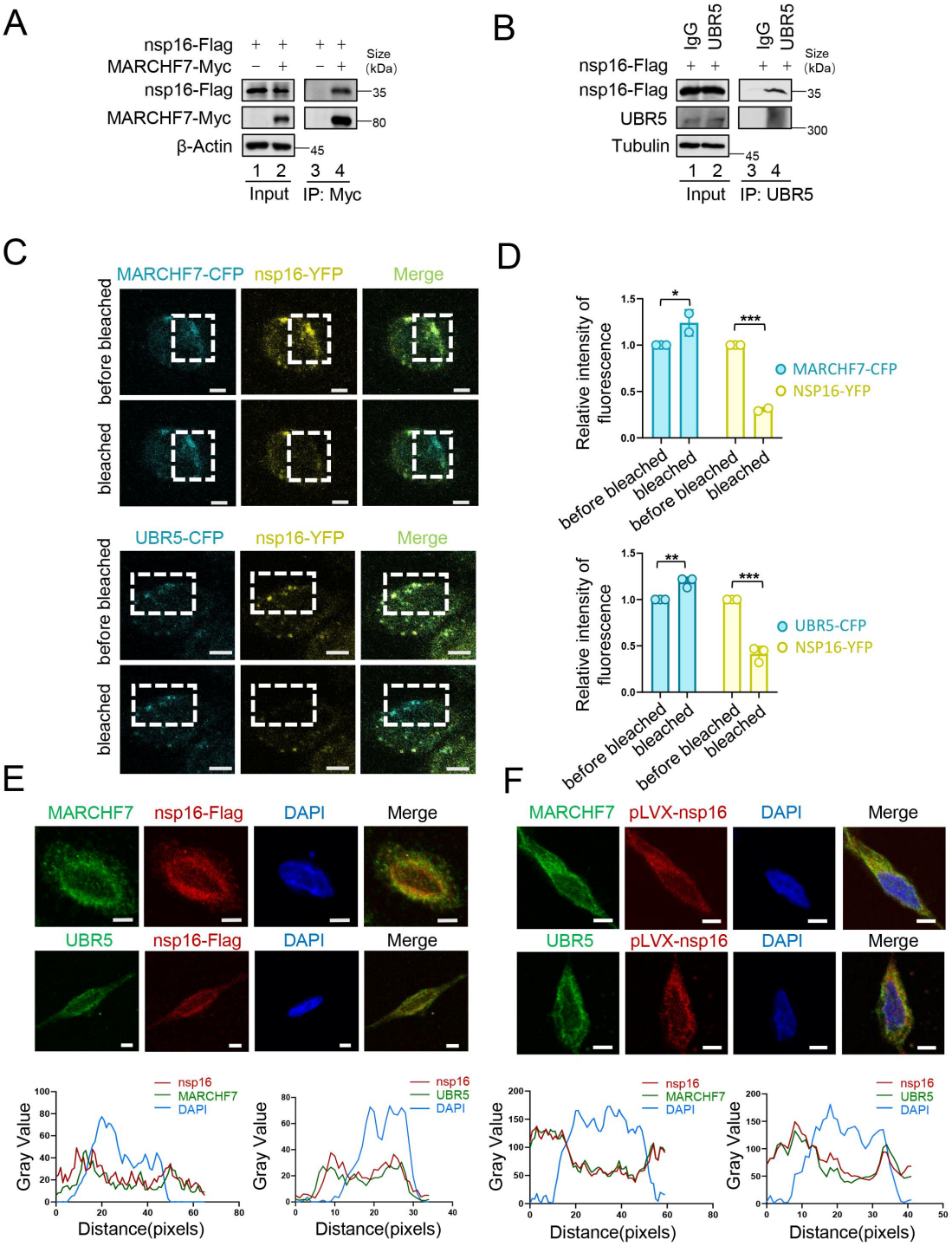

Figure 4 supplement 2

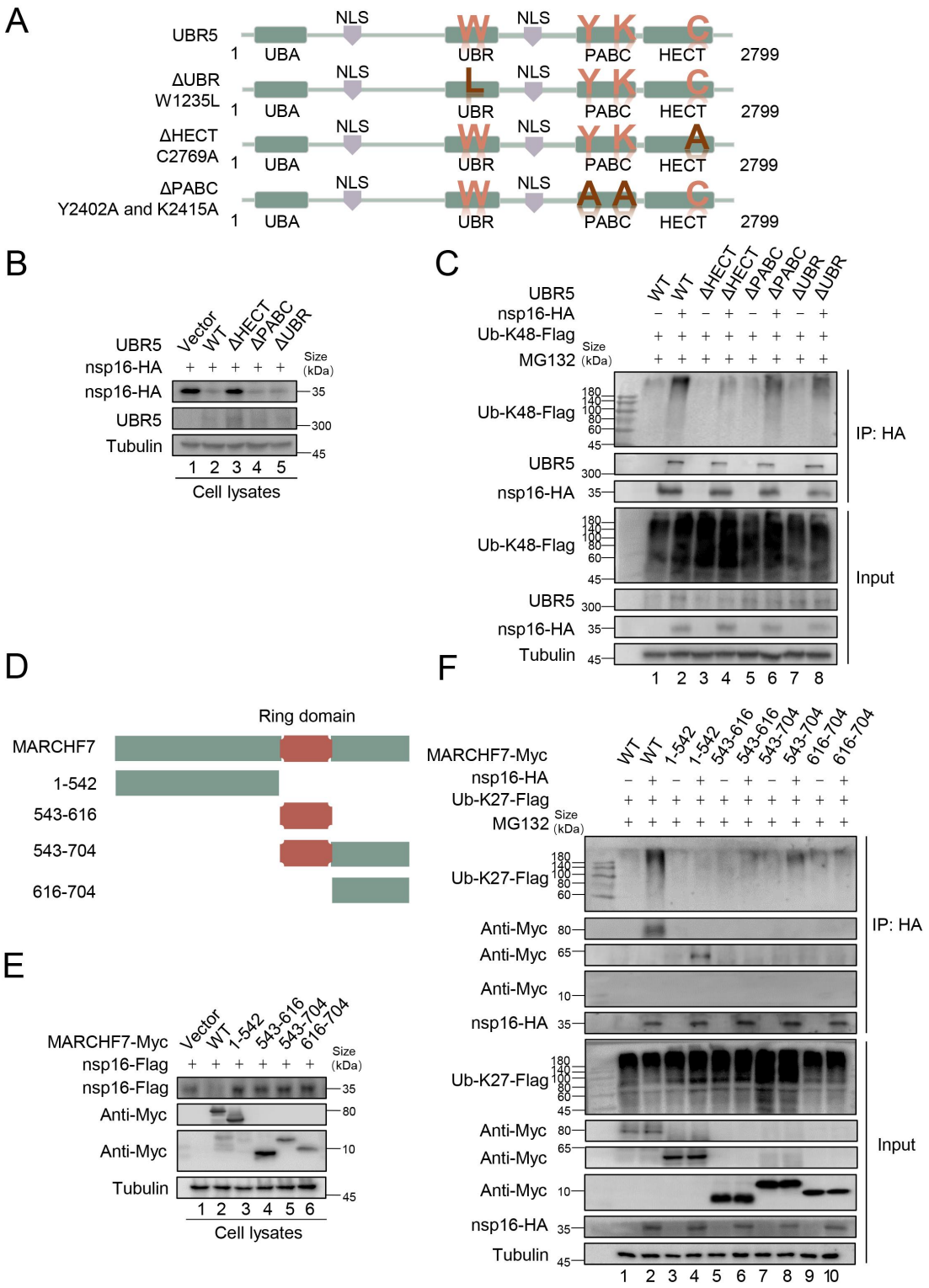

Figure 5

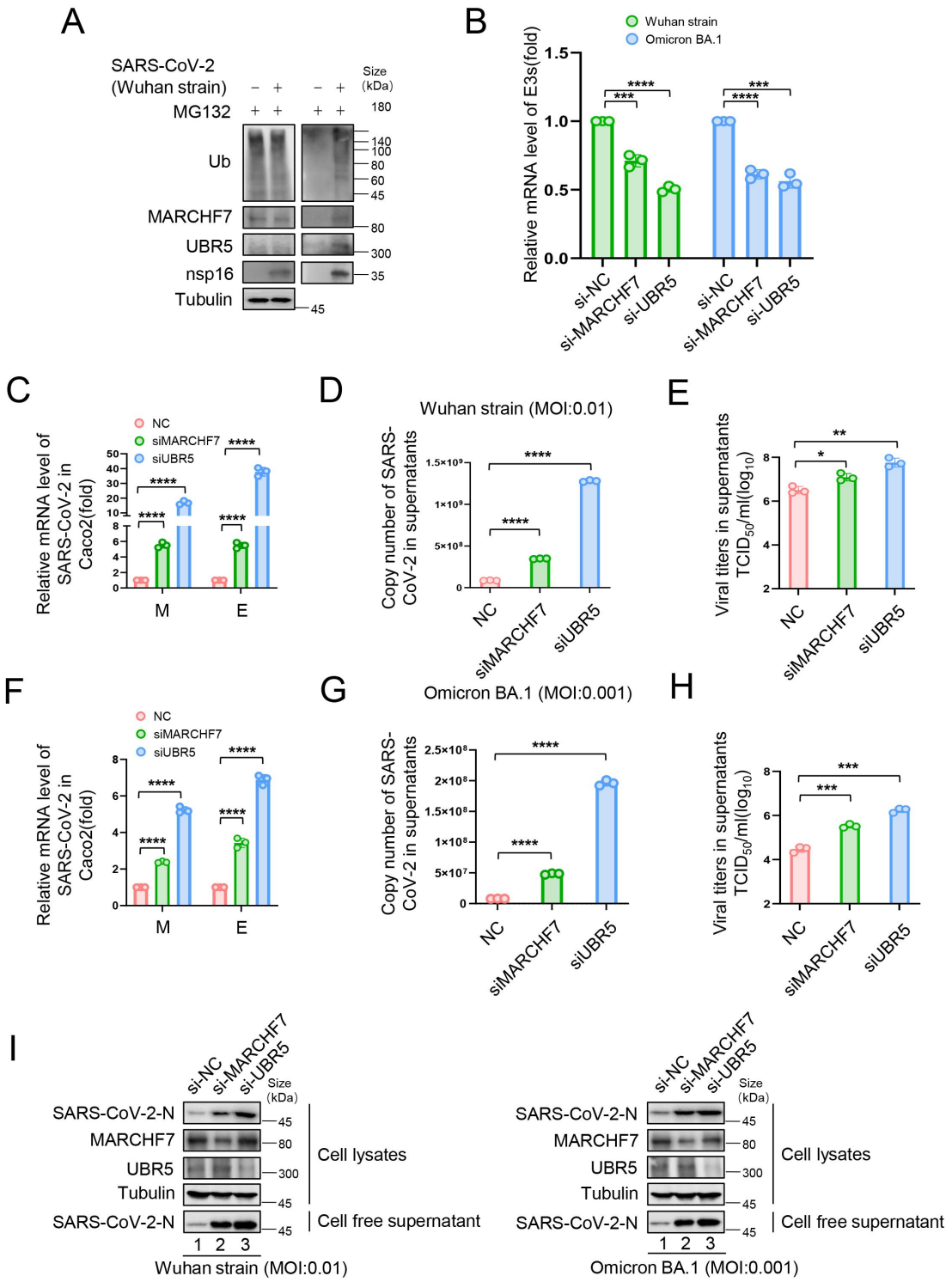
A
SARS-CoV-2 (Wuhan strain)
MG132
Size (kDa)
Ub
MARCHF7
UBR5
nsp16
Tubulin
B
Wuhan strain
Omicron BA.1
Relative mRNA level of E3s(fold)
si-NC
si-MARCHF7
si-UBR5
C
NC
siMARCHF7
siUBR5
Relative mRNA level of SARS-CoV-2 in Caco2(fold)
M
E
D
Wuhan strain (MOI:0.01)
Copy number of SARS-CoV-2 in supernatants
E
Viral titers in supernatants TCID50/ml(log10)
F
Omicron BA.1 (MOI:0.001)
G
H
I
SARS-CoV-2-N
Cell lysates
Cell free supernatant
Wuhan strain (MOI:0.01)
Omicron BA.1 (MOI:0.001)

Figure 5 supplement 1

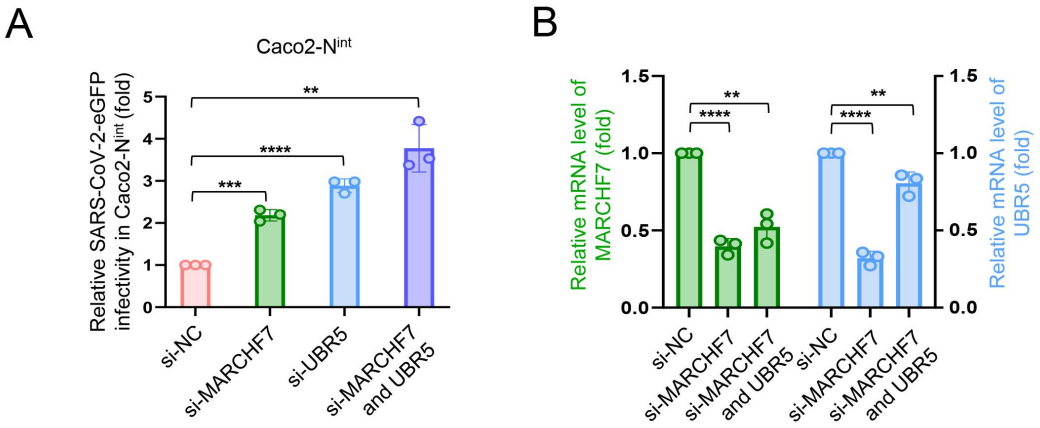

Figure 6

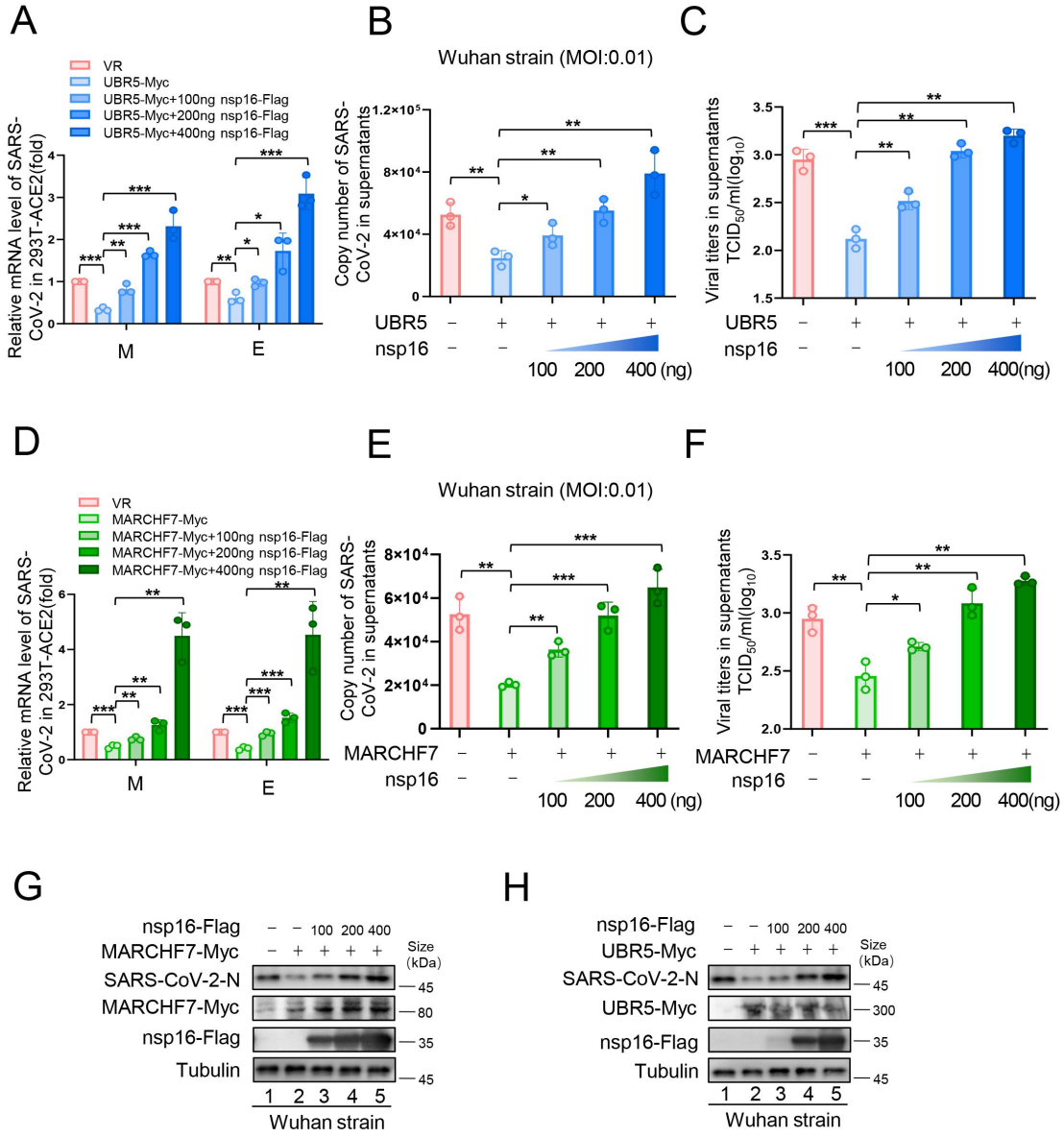
A
VR
UBR5-Myc
UBR5-Myc+100ng nsp16-Flag
UBR5-Myc+200ng nsp16-Flag
UBR5-Myc+400ng nsp16-Flag
Relative mRNA level of SARS-CoV-2 in 293T-ACE2(fold)
M
E
B
Wuhan strain (MOI:0.01)
Copy number of SARS-CoV-2 in supernatants
UBR5
nsp16
100 200 400 (ng)
C
Viral titers in supernatants TCID50/ml(log10)
UBR5
nsp16
100 200 400(ng)
D
VR
MARCHF7-Myc
MARCHF7-Myc+100ng nsp16-Flag
MARCHF7-Myc+200ng nsp16-Flag
MARCHF7-Myc+400ng nsp16-Flag
Relative mRNA level of SARS-CoV-2 in 293T-ACE2(fold)
M
E
E
Wuhan strain (MOI:0.01)
Copy number of SARS-CoV-2 in supernatants
MARCHF7
nsp16
100 200 400 (ng)
F
Viral titers in supernatants TCID50/ml(log10)
MARCHF7
nsp16
100 200 400(ng)
G
nsp16-Flag
MARCHF7-Myc
SARS-CoV-2-N
MARCHF7-Myc
nsp16-Flag
Tubulin
Size (kDa)
Wuhan strain
H
nsp16-Flag
UBR5-Myc
SARS-CoV-2-N
UBR5-Myc
nsp16-Flag
Tubulin
Size (kDa)
Wuhan strain

Figure 6 supplement 1

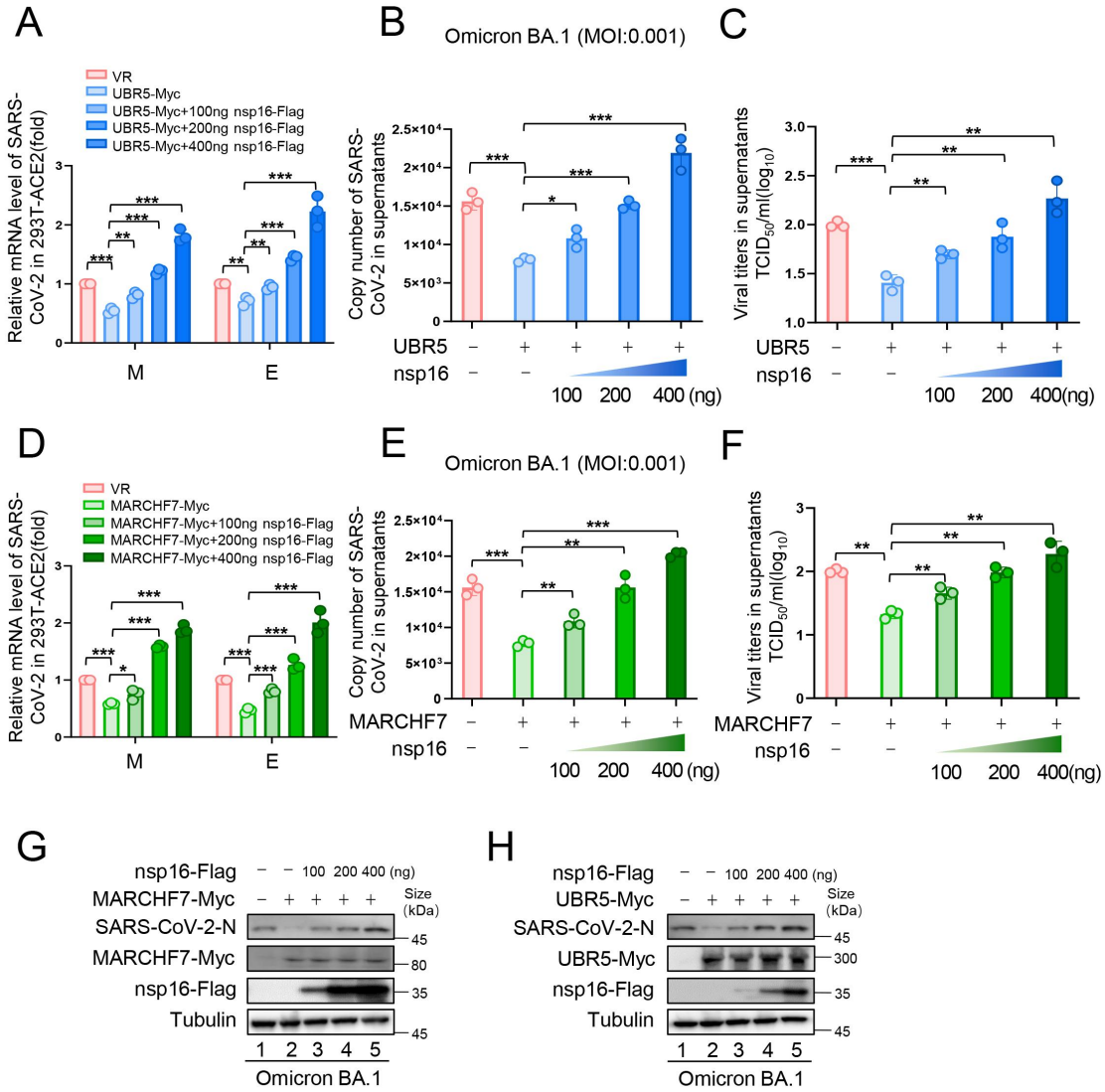

Figure 6 supplement 2

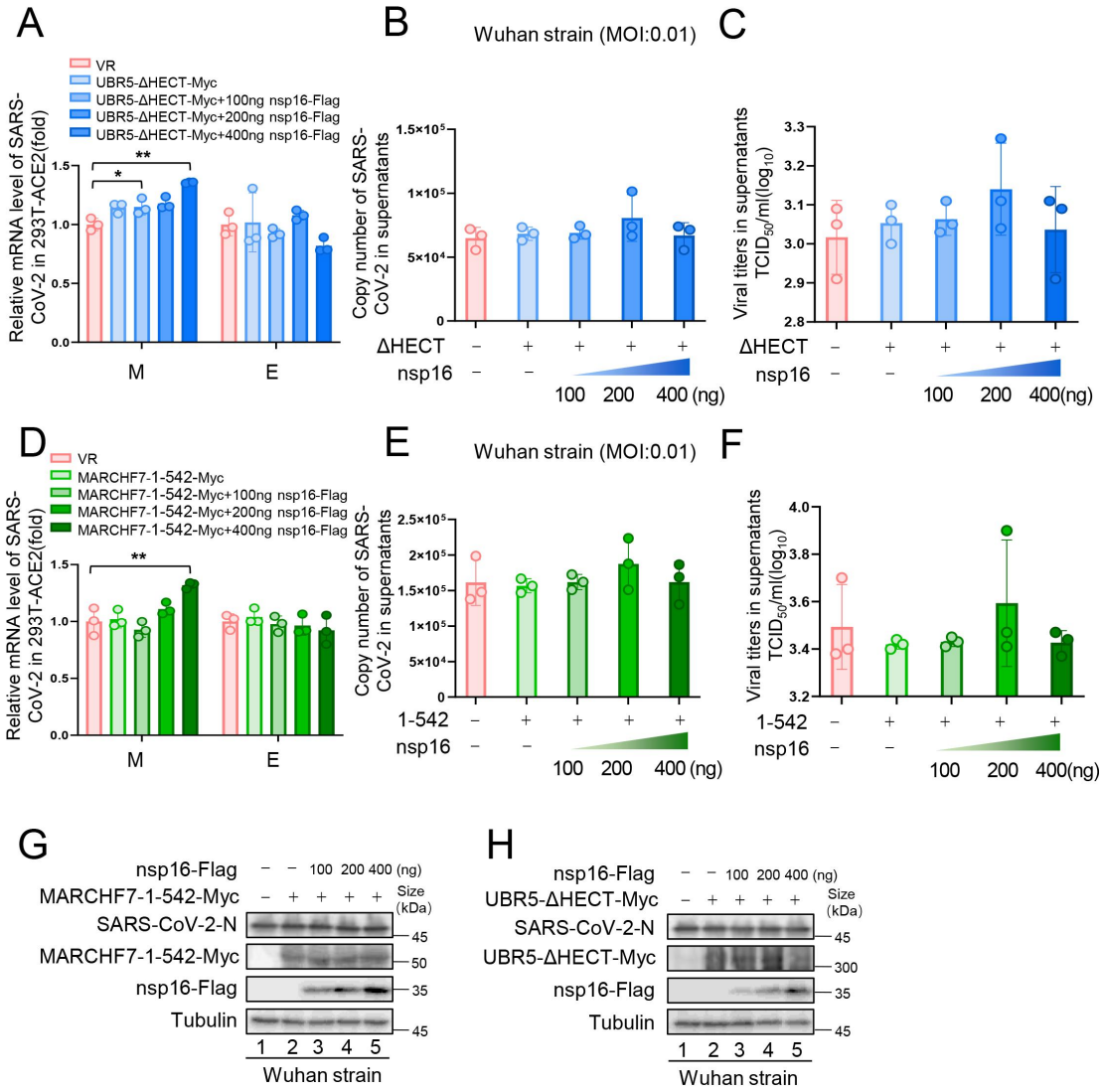

Figure 6 supplement 3

A

	2	9	28	33	34	56	60	68	86	92	93	126	140	142	149	157	160	163	166	167	168	186	215	216	217	232	236	238	252	263	267	269	281	288	289	290	291
WT	S	V	Q	S	A	T	A	I	R	G	T	L	T	E	F	I	K	L	S	V	A	H	P	R	E	R	P	Q	P	K	I	D	I	V	V	I	S
XBB.1.16						I			K								R									/			/		T						
XBB.1.17.1																																	V				
XBB.1.34																																			F		
XBB.1.35													I																								
XBB.1.5				N	V		S	V							/		/		P	A		Y	L								T						P
XBB.1.5.1																					V																
XBB.1.5.10		F																																			
XBB.1.5.15																T																					
XBB.1.5.2	N																																				
XBB.1.5.25																	R																				
XBB.1.5.29					V																																
XBB.1.5.48																												H									
XBB.1.5.61																																G					
XBB.1.5.63																											L										
XBB.1.5.66																		F																			
XBB.1.5.7																																				V	
XBB.1.9.1			K								A			K	/								L	N	V					R				A			
XBB.2.3.2										/																											
XBB.2.3.5																								N													
XBB.2.6												F																									

B

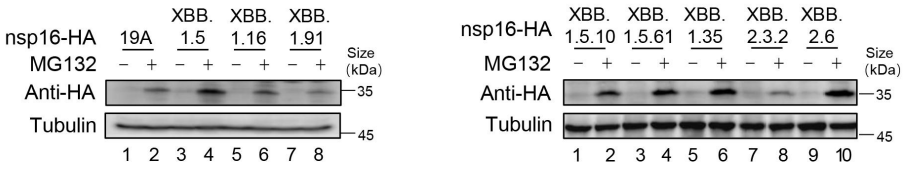

C

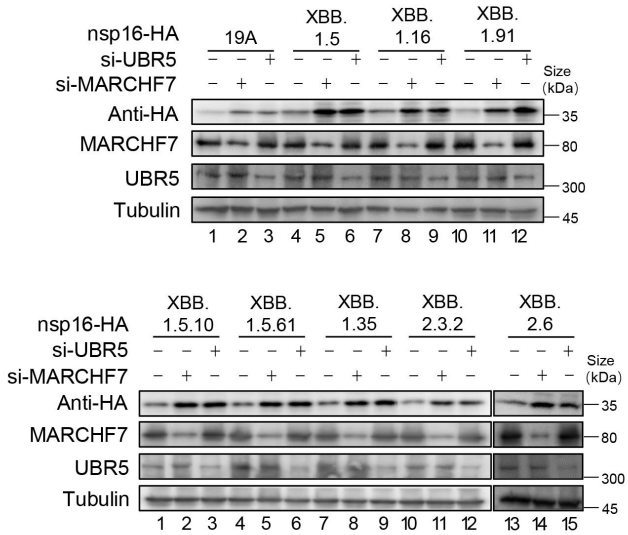

Figure 6 supplement 4

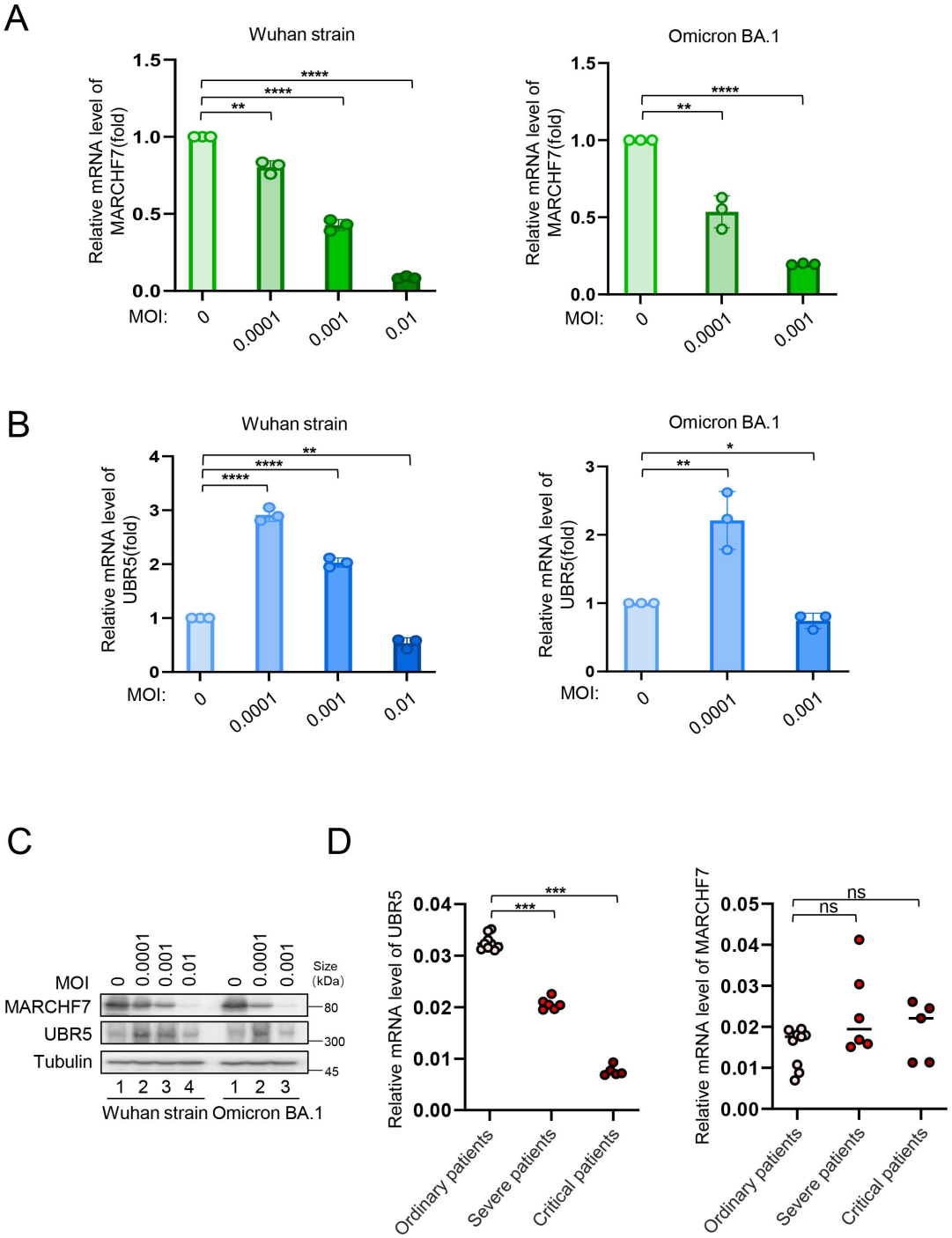

Figure 7

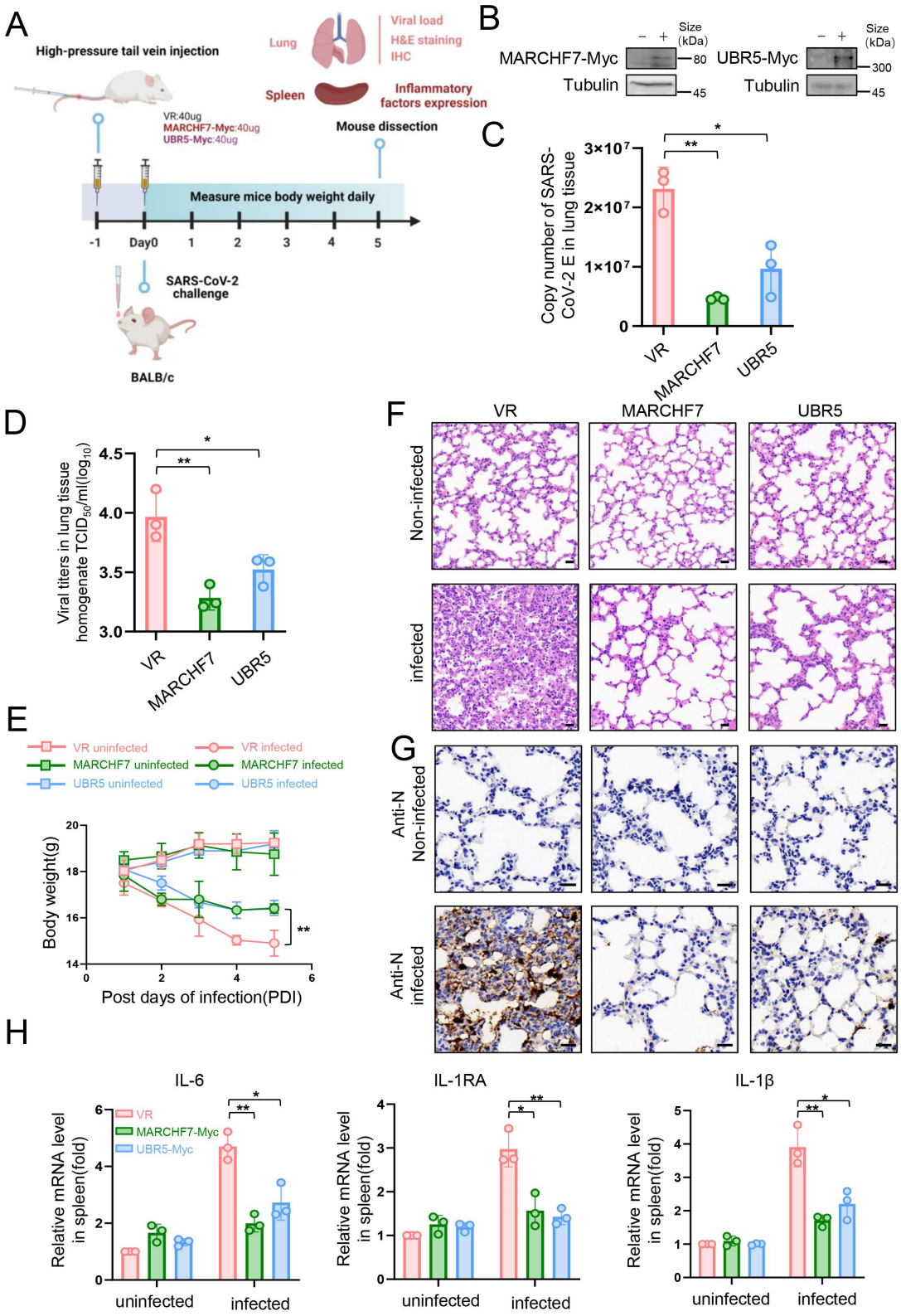
A
High-pressure tail vein injection
VR:40ug
MARCHF7-Myc:40ug
UBR5-Myc:40ug
Lung
Viral load
H&E staining
IHC
Spleen
Inflammatory factors expression
Mouse dissection
Measure mice body weight daily
-1
Day0
1
2
3
4
5
SARS-CoV-2 challenge
BALB/c
B
MARCHF7-Myc
Tubulin
UBR5-Myc
Size (kDa)
80
45
300
C
Copy number of SARS-CoV-2 E in lung tissue
VR
MARCHF7
UBR5
D
Viral titers in lung tissue homogenate TCID50/ml(log10)
E
VR uninfected
VR infected
MARCHF7 uninfected
MARCHF7 infected
UBR5 uninfected
UBR5 infected
Body weight(g)
Post days of infection(PDI)
F
Non-infected
infected
G
Anti-N Non-infected
Anti-N infected
H
IL-6
IL-1RA
IL-1β
Relative mRNA level in spleen(fold)
uninfected
infected

Figure 8

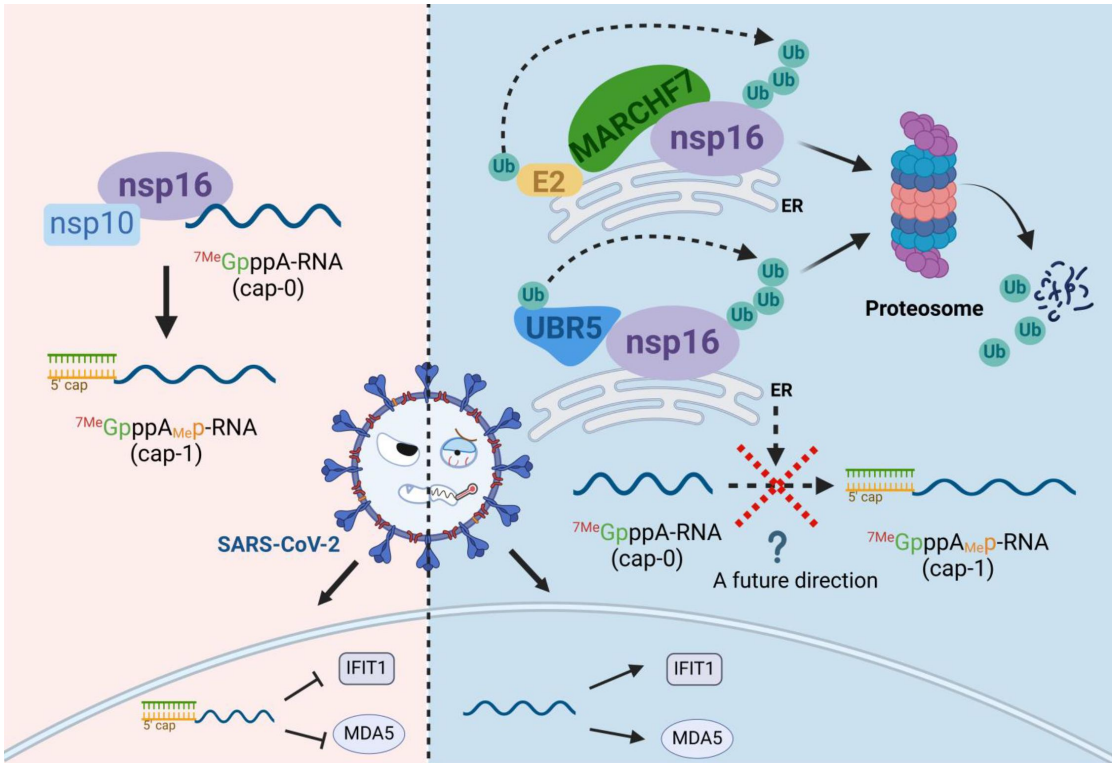
nsp16
nsp10
7MeGpppA-RNA
(cap-0)
5' cap
7MeGpppAMeP-RNA
(cap-1)
SARS-CoV-2
IFIT1
MDA5
5' cap
MARCHF7
nsp16
E2
Ub
ER
UBR5
nsp16
Proteosome
7MeGpppA-RNA
(cap-0)
A future direction
7MeGpppAMeP-RNA
(cap-1)
IFIT1
MDA5